UNCLASSIFIED

Security Classification

AD 748433

DOCUMENT CONTROL DATA - R & D

(Security classification of title, body of abstract and indexing annotation must be entered when the overall report is classified)

ORIGINATING ACTIVITY (Corporate author)	2a. REPORT SECURITY CLASSIFICATION
MARTIN MARIETTA CORPORATION, RIAS DIVISION 1450 SOUTH ROLLING ROAD BALTIMORE, MARYLAND 21227	UNCLASSIFIED 2b. GROUP

3. REPORT TITLE

EXACT SOLUTIONS FOR LIFTING SURFACES

4. DESCRIPTIVE NOTES (Type of report and inclusive dates)

Scientific Interim

5. AUTHOR(S) (First name, middle initial, last name)

PETER F JORDAN

6. REPORT DATE	7a. TOTAL NO. OF PAGES	7b. NO. OF REFS
Aug 1972	46	8

8a. CONTRACT OR GRANT NO.	9a. ORIGINATOR'S REPORT NUMBER(S)
F44620-69-C-0096	RIAS TR 72-17c
b. PROJECT NO. 9781-02	
c. 61102F	9b. OTHER REPORT NO(S) (Any other numbers that may be assigned this report) AFOSR - TR - 72 - 1737
d. 681307	

10. DISTRIBUTION STATEMENT

Approved for public release; distribution unlimited.

11. SUPPLEMENTARY NOTES	12. SPONSORING MILITARY ACTIVITY
TECH, OTHER	AF Office of Scientific Research (NAM) 1400 Wilson Boulevard Arlington, Virginia 22209

13. ABSTRACT

The obstacle which has prevented the determination of exact lifting surface solutions was the singularity at the wing tip. This problem has now been solved analytically for the circular wing and thereby, to an extent, for wings with parabolic wing tips in general. The paper reports the analytical results. It describes how numerical solutions for the circular wing can conveniently be calculated if only engineering accuracy is required. Four linearly independent solutions have been determined to very high accuracy and are listed in tables; the tables are short since it is possible to split off the singularity. The samples confirm some expected and provide some unexpected insights into the mechanism of lifting flow.

DD FORM 1 NOV 65 1473

UNCLASSIFIED

Security Classification

14 KEY WORDS	LINK A		LINK B		LINK C	
	ROLE	WT	ROLE	WT	ROLE	WT
LIFTING SURFACE THEORY (SUBSONIC)						
PARABOLIC WING TIPS						
CIRCULAR WING (EXACT SOLUTION)						
MECHANISM OF LIFTING FLOW						
SLENDER WINGS						
NUMERICAL EXTRAPOLATION						
MATCHING OF SOLUTIONS						
CIRCULAR WING (SIMPLIFIED SOLUTION)						

II

EXACT SOLUTIONS FOR LIFTING SURFACES

P. F. Jordan*

RIAS, Martin Marietta Corp., Baltimore, Md.

The obstacle which has prevented the determination of exact lifting surface solutions was the singularity at the wing tip. This problem has now been solved analytically for the circular wing and thereby, to an extent, for wings with parabolic wing tips in general. The paper reports the analytical results. It describes how numerical solutions for the circular wing can conveniently be calculated if only engineering accuracy is required. Four linearly independent solutions have been determined to very high accuracy and are listed in tables; the tables are short since it is possible to split off the singularity. The samples confirm some expected and provide some unexpected insights into the mechanism of lifting flow.

Research here reported was sponsored by the Air Force Office of Scientific Research (AFSC), United States Air Force, under Contract F44620-69-C-0096.

* Principal Research Scientist

1. Introduction

A great deal of work has been and is being done, many papers have been published, and many computer programs are available concerned with calculating pressure distributions over lifting wings of finite aspect ratio. Nevertheless, the state of the art is not satisfactory. New approaches continue to be proposed, not only because of various complications in the wing model, but largely due to inherent difficulties which arose from singularities in the mathematical formulation of the problem. Consider here only the basic engineering model, the thin lifting surface in steady linear subsonic (hence, by the Prandtl-Glauert transformation, incompressible) flow. No exact solution for any problem of this type has been available. Available numerical methods are approximative collocation methods. The agreement between calculated result and experiment is often satisfactory; on the other hand, there are exceptions. Then, in the absence of an exact solution for the necessarily idealized model of the analysis, there is no criterion by which to determine if the fault lies with either the idealizations in the model or the inaccuracies of the collocation method. The temptation is to blame the model, but divergencies continue to occur in, and between, collocation analyses for a given model. Hence efforts to improve collocation analysis continue.

The present paper does not deal with collocation analyses. Its purpose is to make exact solutions readily available--not exact solutions for all possible engineering models, of course, but exact solution for the basic model in the shape of a circular wing. These solutions describe the pressure singularity that arises on a parabolic tip of a wing of any aspect ratio (one of the hitherto unresolved fundamental problems of potential flow theory) but they are useful beyond this somewhat academic point. They can be used to check the reliability of a given collocation method. They can also provide, sometimes by means of a very brief and straightforward calculation, reliable insights into the mechanism of lifting flow which would be very difficult and cumbersome to derive convincingly with a collocation analysis. To an extent, they can be

generalized to other wing planforms. Furthermore, they allow one to calculate the initial vortex trail exactly.

Our exact solution is based on a formulation by Kinner[1] which has been available since 1937. Prandtl had pointed out that the then new acceleration potential approach would permit one to obtain exact solutions (it no longer required a priori assumptions about the shape of the trailing vortex sheet). The circular wing in incompressible flow appeared to be a suitable model. Kinner[2] formulated the analysis and succeeded in determining overall lift and moment. However, the Kinner results appear to diverge toward the wing tips, and the formulation appeared to be too cumbersome to be of much practical value.

Actually, solutions of the Kinner formulation can readily be calculated to considerable accuracy by solving a relatively simple linear system. The truncated infinite set of numbers which one obtains converges to zero only slowly. The bulk of this set describes the solution for the planar wing (this solution we have chosen as our reference solution; its chief characteristic is the wing tip singularity). With any other solution, the part which is of primary engineering interest is the pressure distribution over the inner part of the wing; this distribution is contained in the void set, that part of the numerical set which is void of the tip singularity. This void set converges much more rapidly.

The analysis by which the details of the structure of the exact solution were derived has been described elsewhere[2-5]. The leading terms[2] were used[3] to calculate the initial shape of the vortex trail (and thus to indicate necessary corrections to earlier analyses). The complete solution is described in Ref. 4; certain results of more general mathematical interest are presented in Ref. 5.

In Section 2 of this paper, the here relevant results of the analysis are reported. In Section 3, the numerical methods are described by which we have calculated the reference solution to a very high accuracy; though this accuracy is not normally required, it serves to demonstrate the details of its structure.

Further accurate solutions, obtained with relative ease once the reference solution is known, are presented and discussed in Section 4.

An alternative simplified approach, useful if one is interested in the solution over the inner part of the wing rather than in the tip singularity, is presented in Section 5. Sample pressure distributions are discussed in Section 6.

The methods here presented allow one to investigate a wide variety of problems of technical interest. The present paper is confined to cases where the given downwash is symmetric and does not contain camber. However, this specialization is not essential.

2. Analytical Results

(a) Pressure Distribution

We describe the pressure difference p between lower and upper wing surfaces by a non-dimensional pressure function $\bar{p}$. From $\bar{p}$ the singularities in p of orders $\pm\frac{1}{2}$ at the leading edge (l. e.) and the trailing edge (t. e.) have been removed:

$$\bar{p} = (1-\xi^2)^{\frac{1}{2}} p/q \qquad (2.1)$$

Here q is the dynamic pressure and the local chordwise coordinate such that $\xi_{l.e.} = -1$, $\xi_{t.e.} = +1$.

The given boundary condition is the downwash wV on the wing. V is the forward speed, $w = \tan\alpha$, α the local incidence. Consider the two limit cases for which solutions are known, the infinite uniform wing (2-D; the two-dimensional case) and the slender wing (s.w.), specifically here the elliptic s.w. in the limit $k \to 0$, where k the axis ratio of the ellipse. The nature of the chordwise distribution $\bar{p}(\xi)$ differs distinctly between these two limits. Assume w constant, and normalize to w=1. One then has the following comparison:

	$\bar{p}(\xi)$	C_ℓ	ξ_ℓ
2-D	$4(1-\xi)$	2π	-0.5
s.w.	$\begin{cases} 4k\lvert\xi\rvert \\ 0 \end{cases}$ if $\begin{cases} \xi \leq 0 \\ \xi \geq 0 \end{cases}$	$2k$	$-\pi/4$

(2.2)

where C_ℓ is the local lift coefficient, ξ_ℓ the local center of pressure.

In 2-D, $\bar{p}(\xi)$ is a polynomial of order (n+1) in ξ if $w(\xi)$ is a polynomial of order n. Such smooth distributions $\bar{p}(\xi)$ we call 2-D type distributions. In contrast, the s.w. distribution has a kink at the wing axis $\xi=0$.

On a wing with finite aspect ratio and with rounded (parabolic) tips, 2-D type distributions must prevail over the inner part of the wing span but the kinked s.w. type must exist at the tip itself. Indeed, this is confirmed by the exact solution. The latter is derived from the Kinner[1] formulation for the distribution of the pressure function $\bar{p}$ over the circular wing:

$$\bar{p}(r,\phi)\tilde{y}/4 = \sum_{k=0}^{\infty} C_{2k} r^{2k} \cos 2k\phi + \sum_{\lambda=0}^{\infty} C_{2\lambda+1} r^{2\lambda+1} \sin(2\lambda+1)\phi \qquad (2.3)$$

Thus $\bar{p}$ is built up from elementary solutions (none of which is physically meaningful individually) with unknown amplitudes C_n. Coordinates and notations in (2.3) are defined in Fig. 1.* In addition to (2.3), we have for $\bar{p}$ the Kutta condition

* Our notation differs somewhat from that of Kinner[1]. Contained in (2.3) is the assumption that the downwash which is given on the wing is both symmetrical and without camber

$$w(\xi, y) \equiv w(y) = w(-y)$$

Kinner[1] shows that, split off in a suitable manner, the camber part $\bar{p}_c$ of a general pressure function is trivial, and zero all along the wing edge. Also, the analysis can readily be rewritten for the case that w(y) is antisymmetric.

$$\bar{p}_{t.e.} \equiv \bar{p}(1, -\pi<\phi<0) \equiv 0 \qquad (2.3a)$$

Integrating (2.3) chordwise, we obtain the local lift coefficient

$$C_\ell(y) = (2\pi/\tilde{y}) \sum_{\kappa=0}^{\infty} C_{2\kappa} P_{2\kappa}(y) \qquad (2.4a)$$

and the local moment coefficient

$$\xi_\ell(y) C_\ell(y) = -\pi \sum_{\lambda=0}^{\infty} (2\lambda+1) C_{2\lambda+1} \bar{P}_{2\lambda}(y) \qquad (2.4b)$$

The $P_{2\kappa}$ are the Legendre polynomials, the $\bar{P}_{2\kappa}$ their derivatives (resp. the ultraspherical or Gegenbauer polynomials)

$$\bar{P}_{2\lambda} = \frac{1}{(\lambda+1)(2\lambda+1)} \frac{d}{dy} P_{2\lambda+1}(y) \qquad (2.4c)$$

Both are symmetrical and orthogonal, normalized such that

$$P_{2\kappa}(\pm 1) = \bar{P}_{2\lambda}(\pm 1) = 1 \qquad (\text{all } \kappa, \lambda) \qquad (2.4d)$$

Integrating also spanwise, one obtains the vector of the total lift

$$C_L = 8C_0 \; ; \; \xi_L = -C_1/3C_0 \qquad (2.4e)$$

It is given by the first two amplitudes alone.

Before turning to the analytical results which arise from combining (2.3) and (2.3a), let us review two graphical presentations of representative results and relate them to (2.2). These results, Figs. 2 and 3, are for our reference case, the planar wing normalized to $w(y) = 1$.

Shown in Fig. 2 is a relief of $\bar{p}$ over the right half wing. Noting the result both of lifting line theory (large span) and of s.w. theory (small span) that the lift distribution over planar elliptic wings is an ellipse, and assuming that this would hold also for the circular wing, we would have $C_\ell = \text{const.} = C_L$. In Fig. 2, $C_L = 1.790\ldots$. Using rounded-off numbers, we would thus expect $\bar{p}_{l.e.} = 4C_L/\pi = 2.28$ from 2-D in (2). The actual $\bar{p}_{l.e.}$ curve in Fig. 2 lies somewhat higher; this is

due, mainly, to the fact that the chordwise distributions $\bar{p}(\xi)$ are not linear (as in (2.2)) but are concave curves. However, they are 2-D type curves as expected, over the inner part of the wing span.

For the wing tip we should have $\bar{p}_{l.e.,tip} = \bar{p}_T = 2C_L = 3.58$ from s.w. in (2.2). The actual value in Fig. 2 is $\bar{p}_T = 3.19$. That this value is distinctly smaller than predicted is not a failure of s.w.. Rather, it turns out that (as was already likely from Ref. 1) the correct lift distribution over planar elliptic wings is not an ellipse.

Additional information about the transition to the tip is provided by the curve for ξ_ℓ, Fig. 3. Over most of the span, ξ_ℓ is not much forward of the $\frac{1}{4}$-chord point $\xi = -0.5$. The transition to the tip value $-\pi/4$, see (2.2), occurs rapidly and with a vertical tangent.

The singularity at the tip which is illustrated by Fig. 3 is not apparent in the curve $\bar{p}_{l.e.}$ of Fig. 2, but a singularity in $\bar{p}$ occurs as the tip is approached along the wing axis $\xi=0$.

A measure for the amplitude of the tip singularity in $\bar{p}$ is the tip value $\bar{p}_T$. For it one finds, considering that due to (2.3a) the two sums in (2.3) must equal each other at the l.e.,

$$\bar{p}_T \equiv \lim_{\phi \to +0} \bar{p}(1,\phi) = 8 \sum_{\lambda=0}^{\infty} (2\lambda+1) C_{2\lambda+1} \qquad (2.5)$$

One also shows that, moving toward the tip along any half-ellipse ξ=const., one reaches

$$\lim_{y \to 1} \bar{p}\ (\xi=\text{const.}) = \begin{cases} |\xi| \bar{p}_T \\ 0 \end{cases} \text{ if } \begin{cases} \xi \leq 0 \\ \xi \geq 0 \end{cases} \qquad (2.5a)$$

This is in agreement with the s.w. distribution $\bar{p}(\xi)$ in (2.2). According to (2.7), the $\bar{p}$ curves of Fig. 2 over the half-ellipses $\xi = -0.8, -0.6, \ldots$ reach the tip vertical at equidistant points $\bar{p} = 0.8\bar{p}_T,\ 0.6\bar{p}_T, \ldots$. All those for $\xi > 0$ reach the same end point $\bar{p}=0$.

Due to (2.4b), the $C_{2\lambda+1}$ may be called the moment amplitudes; according to (2.5), they determine $\bar{p}_T$. For the lift amplitudes $C_{2\kappa}$ we have the zero sum condition

$$\sum_{\kappa=0}^{\infty} C_{2\kappa} = 0 \tag{2.6}$$

Utilizing the orthogonality of the circular functions, one finds from the equality along the l. e. of the two sums in (2.3) that the two sets of amplitudes are fully interdependent and equivalent. Introducing the abbreviation $\bar{\lambda}=(\lambda+\frac{1}{2})$, we have

$$\pi C_{2\lambda+1} = 2 \sum_{\kappa=0}^{\infty} \frac{\bar{\lambda} C_{2\kappa}}{\bar{\lambda}^2 - \kappa^2} \qquad \text{(all } \lambda\text{)} \tag{2.7a}$$

$$\pi C_{2\kappa} = 2 \sum_{\lambda=0}^{\infty} \frac{\bar{\lambda} C_{2\lambda+1}}{\bar{\lambda}^2 - \kappa^2} \qquad \text{(times } \tfrac{1}{2} \text{ if } \kappa=0\text{)} \tag{2.7b}$$

The transformation (2.7b) leads to a set which automatically fulfills (2.6). As an example, set $C_1=1$; $C_{2\lambda+1}=0$ for $\lambda \neq 0$. Then

$$\pi C_0 = 2 \; ; \; \pi C_{2\kappa \neq 0} = -(\kappa^2 - 1/4)^{-1} \tag{2.8}$$

One readily shows that this set fulfills (2.6).

The set (2.8) is one of a sequence of possible elementary sets which one might use to build up the complete solution for a given downwash w(y). Choose an integer λ^* and let

$$C_{2\lambda^*+1} \neq 0 \; ; \; C_{2\lambda+1} = 0 \text{ for } \lambda \neq \lambda^* \tag{2.9}$$

The pressure distribution which results is characterized by its l. e. distribution

$$\bar{p}_{l.e.} = 8 \frac{\sin(2\lambda^*+1)\phi}{\sin\phi} C_{2\lambda^*+1} \tag{2.9a}$$

and is thus a spanwise wavy distribution. We will further discuss the elements λ^* in Section 6.

The elements λ^* are not an optimum choice because one requires an infinite number of them to produce a downwash w(y) which is regular at the wing tip. We generally denote by E_κ any elementary set which we use to build up the solving set $C_{2\kappa}$, and we always require that E_κ individually fulfills the zero sum condition (2.6). From (2.8) arises the suggestion to consider the sets

$$E_0^r = \zeta(r) \; ; \; E_\kappa^r = -\kappa^{-r} \quad (\kappa \neq 0) \tag{2.10}$$

Here ζ denotes the Riemann function, see e.g. Table 23.3 of Ref. 6. We call the sets E_κ^r the rational sets; we will also have to use logarithmic sets.

According to (2.7b), the set E_κ^2 is the leading set. Thus

$$C_{2\kappa} = -\frac{a_2}{\kappa^2} + R_\kappa \qquad (\kappa \neq 0) \tag{2.11}$$

In (2.11), a_2 is an unknown amplitude, and the remainder R_κ is defined by the condition $R = o(\kappa^{-2})$. One can show that R_κ does not contribute to the tip value $\tilde{p}_T$ and thus does not contribute to first order to the tip singularity. Hence we are mainly interested in the elementary pressure function $\tilde{p}_2$ which arises from inserting E_κ^2 into (2.7a) to determine its corresponding set $C_{2\lambda+1}^2$, and then inserting both E_κ^2 and $C_{2\lambda+1}^2$ into (2.3). For $\tilde{p}_2$ we have analytical results for both the l.e. and the wing axis $\beta = 0$:

$$\begin{aligned} \tilde{p}_{2,\,l.e.} &= \frac{8\beta}{\sin\beta}\,(\pi - \beta) \\ \tilde{p}_{2,\,axis} &= 4\left[\zeta(2) - f(\tilde{y}^2)\right]/\tilde{y} \\ &\sim 4\tilde{y}\left[2\log(1/\tilde{y}) + 1 + \tilde{y}^2\log(1/\tilde{y}) + \ldots\right] \end{aligned} \tag{2.12}$$

The function f here is the dilogaritlum, see, e.g., 27.7 of Ref. 6. The two functions (2.12) exhibit the characteristic properties of $\tilde{p}$ in Fig. 2: a smooth curve along the l.e., a vertical tangent at the tip in $\tilde{p}_{axis}$.

From (2.11) and (2.12) follows $\bar{p}_T = 8\bar{\pi}a_2$. From (2.2) and (2.5a) follows $\bar{p}_T = 2C_\ell(1)$. Hence

$$C_\ell(1) = \bar{p}_T/2 = 4\bar{\pi}a_2 \tag{2.13}$$

(b) Structure of the Solution

We describe the given downwash w(y) by a set of downwash coefficients w_s

$$w(y) = \sum_{s=0}^{\infty} (s+1)(2s+1)w_s \bar{P}_{2s}(y) \tag{2.14}$$

where the $\bar{P}_{2s}(y)$ are the Gegenbauer polynomials of (2.4c) and are subject to the normalization (2.4d). Reversing (2.14) we have

$$w_s = (4s+3)\int_0^1 \left\{ \int_0^y w(\eta)d\eta \right\} P_{2s+1}(y)dy \tag{2.14a}$$

For example, in our reference problem

$$w_0 = 1 \;;\; w_{s\neq 0} = 0 \quad \text{if } w(y)\equiv 1 \tag{2.14b}$$

The relation between the sets w_s and C_{2k} is*

$$w_s = \mathbb{T}C_{2s+1} + S_1(C_{2k}) \tag{2.15}$$

where

$$S_1(C_{2k}) = \frac{1}{2}\sum_{k=1}^{\infty}\left[\frac{1}{\bar{s}(k+\bar{s})} - \frac{1}{(\bar{s}+\frac{1}{2})(k+\bar{s}+\frac{1}{2})}\right]kC_{2k} \tag{2.15a}$$

The set C_{2s+1} is given by (2.7a), with λ replaced by s. The operator S_1 is of higher order; the abbreviation $\bar{s}=s+\frac{1}{2}$ corresponds to $\bar{\lambda}$.

One obtains information about the structure of the set C_{2k} by observing that in all technically meaningful cases the downwash w_s is regular at the tip. From this follows that the set w_s must converge more rapidly than any power of $(1/s)$.

---

* This form is considerably more convenient analytically than the original presentation, Eq. (60) of Ref. 1.

To this requirement we refer as the tip condition for the set w_s.

The C^r_{2s+1} which arise from the E^r_κ and which thereby occur in (2.15) are generally $0(s^{-3})$; hence there have to be certain relations between their amplitudes a_r such that terms of this order (as well as of higher orders) cancel out. The investigation becomes fairly intricate because of the occurrence of logarithmic sets in addition to rational sets; on the other hand, it is these logarithmic sets which enforce certain useful general relations. The result[4] we write here in the form

$$-C_{2\kappa} = \left[\frac{4}{\kappa(4\kappa+1)} - \frac{3\log^2\kappa}{16\pi^2\kappa^4}\right]a_2 + R_\kappa \qquad (2.16)$$

Abbreviating, we write this as

$$-C_{2\kappa} = G_\kappa C_\kappa(1) + R_\kappa \qquad (2.16a)$$

and describe it by saying that $C_{2\kappa}$ is composed of a general set G_κ, common to all solutions, and a remainder set R_κ. For the unknown amplitude $C_\kappa(1)$ of G_κ we have (2.6) with (2.13).

Between (2.11) and (2.16), certain elementary sets E_κ have been transferred, by means of the tip condition for the set w_s, from the remainder R_κ of (2.11) into the general set G_κ. On principle, one could continue this process. However, this would serve no useful purpose. Namely, the remainder R_κ of (2.16) (which differs of course from that of (2.11)) contains, in addition to further general sets, also specific sets which describe the solution for the specific given downwash w(y). The orders of magnitude of the two leading specific sets are $0(\kappa^{-4}\log\kappa)$ and $0(\kappa^{-4})$. There is no practical advantage in knowing general sets which are of higher order than these specific sets (the next general set is presumably $0(\kappa^{-5}\log^2\kappa)$).

We will require also some information about the structure of the sets $C_{2\lambda+1}$. If we rewrite (2.16) in the alternative form

$$-C_{2\kappa} = \left[\frac{1}{\kappa^2} - \frac{1}{4\kappa^3} - \frac{3\log^2\kappa}{16\pi^2\kappa^4}\right]a_2 + R_\kappa \qquad (2.16b)$$

we have again $R_\kappa = 0(\kappa^{-4}\log\kappa)$ and have for large $\bar{\lambda}$

$$\pi C_{2\lambda+1} = \left\{\left[1 + I_\lambda - \log 2\right] a_2 - 2\sum_1^\infty \kappa^2 R_\kappa\right\}/\bar{\lambda}^3 - 3a_2\log\lambda/16\bar{\lambda}^4 + 0(1/\lambda^4) \tag{2.16c}$$

The set L_λ is a logarithmic set which is related to the ψ (digamma) function; it is defined by

$$L_\lambda = 1 + \frac{1}{3} + \frac{1}{5} + \ldots + \frac{1}{2\lambda-1} = \tfrac{1}{2}\left[\psi(s+\tfrac{1}{2}) - \psi(\tfrac{1}{2})\right] \simeq \tfrac{1}{2}\log\lambda \tag{2.16d}$$

(c) Span Loading and Tip Distribution

In order to translate (2.16) resp. (2.16b) into a formula for the lift coefficient $C_\ell(y)$, we need, according to (2.4a), the functions

$$e(y) = \sum_{\kappa=0}^{\infty} E_\kappa P_{2\kappa}(y) \tag{2.17}$$

which are created by the various elementary sets in (2.16). We have analytical results only for the two leading sets[5]

$$e_2(y) = 2\tilde{y} + \tfrac{1}{2}\tilde{y}^2\log(2/\tilde{y}) + O(\tilde{y}^2)$$
$$e_3(y) = \tilde{y}^2\log(2/\tilde{y}) + O(\tilde{y}^2) \tag{2.17a}$$

Using these in (2.4a with (2.16), we obtain

$$C_\ell(y) = \left[1 + (1/8)\tilde{y}\log(2/\tilde{y})\right] C_\ell(1) + O(\tilde{y}) \tag{2.18}$$

A useful application of this formula is illustrated in Fig. 4. Numerical summation of (2.4a) becomes cumbersome near the tip because of the denominator $\tilde{y}$. Shown in Fig. 4 are, near the tip and to a large scale, the approximate curves which have been calculated truncating (2.4a) after N = 20, 25..40 terms. The last two curves have converged well enough to the left, that is, inside $y=\pm 0.96$, but all curves show increasing waviness toward the right and turn up toward $+\infty$ at the tip. This

remains true for all finite N. Also shown is the asymptotic curve, the term with $C_\ell(1)$ of (2.18). To obtain a fairly accurate curve $C_\ell(y)$, one has to match the asymptotic curve with the curve N=40 near y=0.98 and has to smooth out the latter curve between y=0.96 and 0.98.

We insert here an illustration, Fig. 5, of a similar matching process for the chordwise distributions $\bar{p}(\bar{\xi})$ near the wing tip. The curves shown represent the result of using in (2.3) the first N=40 amplitudes of each set, C_{2K} and C_{2K+1} of our reference solution. Again convergence deteriorates as $y \to 1$ because of the denominator $\tilde{y}$. The largest error due to truncation occurs along the wing axis. Here the points due to $\bar{p}_2$ alone, see (2.12), are shown as circles.

When y=0.980, curve and point almost coincide. The truncation error is still small, and the leading contribution $\bar{p}_2$ still almost equals the total. As y is increased, the latter becomes increasingly more correct while the truncation errors increase. The slight waviness in the curve for y=0.995 is presumably not genuine but due to truncation errors.

Both Fig. 3 and Fig. 5 show that the transition from the kinked tip distribution to the smooth 2-D type distributions occurs rather rapidly.

With Fig. 6 we return to span loadings. The reference planar solution is shown, and all other curves are normalized to its tip value $C_\ell(1)$. Illustrated is the role of the leading terms in (2.16). The curve $C_\ell^2(y)$ represents the contribution of E_K^2; in it, the factor (1/8) of (2.18) is replaced by (1/4), see (2.17a), and accordingly it cuts over the correct curve near the tip.

The downwash which belongs to E_K^2 is shown in Fig. 7, denoted as w_2. It is negative infinite at the tip; that of the elliptic lift distribution, not shown in Fig. 7, is positive infinite at the tip.

In Figs. 6 and 7, basic refers to the simplest set C_{2K} which produces a finite value w(1):

$$-C_{2K,\,\text{basic}} = \left[\frac{1}{K^2} - \frac{1}{4K^3} + \frac{\bar{a}_4}{K^4}\right] a_2 \qquad (2.19)$$

The first two terms on the right cancel between them a term $0(s^{-3}\log s)$ in w_s (and produce the correct factor $(1/8)$ of (2.18)). Their combined downwash is shown in Fig. 7. The third term in (2.19) is added to cancel also the term $0(s^{-3})$ in w_s. The amplitude $\tilde{a}_4$ which achieves this is

$$\tilde{a}_4 = \frac{10 + \zeta(2)}{16\zeta(2) + 4\zeta(3)} = 0.3741083\ldots \qquad (2.19a)$$

The basic downwash curve in Fig. 7 is seen to be almost a horizontal line, but it has an infinite tangent at the tip. The curve basic in Fig. 6 goes asymptotically into the planar curve at the tip.

The point marked collocation analysis in Fig. 6 is determined from numerical results[7], calculated by means of an unusually careful spanwise integration. The collocation results coincide with the correct planar curve over the inner part of the wing span. It deviates at the tip by 5.4%; this deviation arises because collocation analyses assume an elliptic type lift distribution and thus a finite slope in the $C_\ell(y)$ curve at a parabolic wing tip.

The pressure formula (2.3) and the result (2.16) are specific to the circular wing, but insofar as (2.16) can be translated into the analytical form (2.18), it can be generalized to apply to arbitrary wings with parabolic wing tips[4]. For such wings the local lift becomes

$$\ell(y) = \left\{\left[1 + \frac{\tilde{y}}{16}\left(\frac{b}{2r}\right)^{\frac{1}{2}}\log\frac{8r}{\tilde{y}^2 b}\right] C_\ell(1) + R(y)\right\} c(y) q \qquad (2.20)$$

Here b is the wing span, r the wing tip radius, c(y) the wing chord. The remainder function R(y) may be expected to have a finite tangent at the wing tip.

3. Numerical Procedure

For a given downwash w(y) one finds the set w_s by means of (2.14a) and has in (2.15) an infinite linear system for calculating the set C_{2k}. Solving this system after truncating it to N equations, one obtains N values C_{2k}^N which represents

a truncated approximation to the correct set $C_{2\mu}$.

Convergence toward the correct set $C_{2\mu}$ slows down as N is increased because the set $C_{2\mu}$ itself, being a reciprocal progression, converges with increasing slowness as $\mu \to \infty$. To improve the convergence, one calculates first the set $C_{2\lambda+1}$. For this purpose (2.15) is rewritten as

$$w_s = \pi \sum_{\lambda=0}^{\infty} c_\lambda^s C_{2\lambda+1} = \pi C_{2s+1} - \frac{1}{\pi} \sum_{\lambda=0}^{\infty} \bar{c}_\lambda^s C_{2\lambda+1} \tag{3.1}$$

The matrix c_λ^s is almost the unit matrix; the numbers $\bar{c}_\lambda^s$ (which correspond to the operator S_1 in (2.15)) are small. A short numerical table follows:

s \ λ	0	1	2	3
0	0.9112	-0.0470	-0.0315	-0.0236
1	-0.0117	0.9902	-0.0078	-0.0064
2	-0.0039	-0.0041	0.9964	-0.0032
3	-0.0018	-0.0021	-0.0021	0.9981

c_λ^s

The $\bar{c}_\lambda^s$ are given by

$$\begin{aligned} \bar{c}^s &= MS - (M-N)L_{s,\lambda} && \text{if } \lambda \neq s \\ &= T - \left[4\bar{s}/(4\bar{s}+1)\right]S && \text{if } \lambda = s \end{aligned} \tag{3.2}$$

Here

$$M = \bar{\lambda}/(\bar{\lambda}^2-(s+1)^2) \quad ; \quad N = \bar{\lambda}/(\bar{\lambda}^2-\bar{s}^2)$$

$$L(s,\lambda) = 2L_\lambda + (1/2\bar{\lambda}) - (1/2\bar{s}) - 2L_s$$

$$S = 2\log 2 - \sum_{\nu=1}^{s} \frac{1}{(2\nu-1)} - \frac{1}{2(2s+1)(s+1)} \tag{3.2a}$$

$$T = (\pi^2/4) - \sum_{\nu=1}^{s} \frac{2}{(2\nu-1)^2} - \frac{1}{(2s+1)^2}$$

The set L_s is defined by (2.16d).

Having calculated the set $C^N_{2\lambda+1}$ using a truncated system (3.1), one uses (2.7b) to calculate the corresponding truncated set $C^N_{2\kappa}$.*

The complete procedure is easily programmed for digital computation**. No large number N is required to obtain engineering accuracy. One obtains an accuracy of about 10^{-7} with N=40 in the reference problem (2.14b); of course, the accuracy goes down, or N has to be increased, if higher coefficients w_s occur. With N=40, one has more than sufficient accuracy for most purposes over the inner part of the wing. If one wants to match near the tip, as in Figs. 4, 5, one needs also the amplitude a_2 of the tip singularity. If no unusual accuracy is required, it is sufficient to assume that $R_\kappa=0$ in the highest $C^N_{2\kappa}$ which have been calculated; then a_2 is obtained directly from (2.16).

4. Calculation of the Reference Solution

(a) Approach

We have determined the reference solution plus three further solutions to very high accuracy in order to definitely determine and demonstrate the details of the structure of the solutions (and also the powerfulness of the available methods). We used up to N=60 equations, used 12 decimals in the results to extrapolate to N=∞, lost 2 decimals in the extrapolations and performed the further calculations with 10 decimals. The resulting sets $C_{2\kappa}$ are listed in Tables I and II, rounded to 8 decimals.

---

* The $C^N_{2\kappa}$ which are calculated directly from (2.15) decrease as N is increased; those calculated via (3.1) and (2.7b) increase with N. The two different results thus establish reliable (though not overly narrow) bounds.

** A program for the UNIVAC 1108 which delivers both $C^N_{2\lambda+1}$ and $C^N_{2\kappa}$, with N a variable, can be obtained from the author.

It is easy to extrapolate to N=∞ results which converge like geometric series. In the present problem behavior like reciprocal powers of N was more likely (see Appendix E of Ref. 8) and was in fact indicated by the numerical results. For the $C_{2\lambda+1}$, we used successfully the following principle: Assume

$$f(N) = f(\infty) - A/N^r \qquad (4.1)$$

where A and r are unknown constants. Then to second order

$$2\Delta(N) = f(N+1) - f(N-1) = 2rA/N^{r+1}$$

Thus

$$\frac{\Delta(N)}{\Delta(M)} = (M/N)^{r+1}$$

from which one finds r, and

$$f(\infty) = f(N) + N\Delta(N)/r$$

The point now is that, while we do not know if (4.1) correctly describes the dependency of $C^N_{2\lambda+1}$ on N, the same procedure works fairly well if the term on the right should be $A\log N/N^r$, for example. In fact, this seemed to be the case, with r of the order r=3. By performing the evaluation with several values M, one obtains information about the validity of the assumption made and about the accuracy of the resulting value f(∞).

The set $C_{2\kappa}$ required a modified approach to be described below. The final set $C_{2\lambda+1}$ was used to determine the ampoitude $C_\ell(1)$ of the tip singularity.

(b) Outer Solution

We call the amplitude $C_\ell(1)$ the outer solution; it has to be determined by a matching process. The difficulty of matching in terms of $C_\ell(y)$ is illustrated by Fig. 4. A more definite approach is provided by the sum condition (2.5), which we write here in the form

$$C_\ell(1) = S(N) + \Delta(N) = 4\sum_0^N (2\lambda+1)C_{2\lambda+1} + 4\sum_{N+1}^{\infty} (2\lambda+1)C_{2\lambda+1} \qquad (4.2)$$

One visualizes that one could calculate S(N) for a number of values N, plot these over u=(1/N), and extrapolate to the origin u=0. The end value of the extrapolation

curve would then be $C_\ell(1)$. However, we know from (2.16c) that the leading elements in the set to be summed have the form

$$(2\lambda+1)C_{2\lambda+1} = \frac{D_0 \log\lambda + D_1}{(2\lambda+1)^2} + \frac{D_2 \log\lambda + D_3}{(2\lambda+1)^3} + \ldots \qquad (4.3)$$

Therefore $\Delta(N)$ behaves like ulogu; S(N), plotted over u, will have a vertical tangent, and extrapolation is unreliable.

To eliminate this difficulty, replace (4.2) by

$$C_\ell(1) = S^*(N) + \Delta^*(N) \qquad (4.4)$$

with

$$S^*(N) = S(N) + 4N(2N+1)C_{2N+1} \qquad (4.4a)$$

Then, using formula (A4) of the Appendix

$$\Delta^*(N) = \frac{4N+3}{(2N+1)^2} D_0 - \left[(\log N - \tfrac{1}{2})D_2 + D_3\right] \frac{2N}{(2N+1)^3} + \ldots \qquad (4.4b)$$

The coefficient D_1 has disappeared from the leading terms, and the curve S*(N) has the form $C_\ell(1) - O(u)$. This curve was used in Ref. 2. It is shown at the far left of Fig. 8; the error in its end value $C_\ell(1)$ was about 10^{-5}.

The marked improvement which is illustrated by the two main curves of Fig. 8 is due to matching with new analytical results[4]. According to (2.16c)

$$D_0 = C_\ell(1)/\pi^2 \quad ; \quad D_2 = -3C_\ell(1)/4\pi^2 \qquad (4.5)$$

Inserting at first only D_0 into (4.4b), we replace (4.4) by

$$C_\ell(1) = S^*(N)/\left[1 - \frac{4N+3}{\pi^2(2N+1)^2}\right] + \frac{a \log N - b}{(2N+1)^2} + \ldots \qquad (4.6)$$

with constants a and b. The first term on the right we denote by S*/[ ]. Its curve in Fig. 8 has to have a horizontal tangent at its origin $C_\ell(1)$.

The lower curve in Fig. 8 has been constructed using the original sets $C^N_{2\lambda+1}$ rather than the extrapolated set; this curve must reach the correct origin $C_\ell(1)$ but we do not know if it has to have a horizontal tangent.

The upper curve was calculated using the final set $C_{2\lambda+1}$, up to N=40. (Accuracy deteriorates when N becomes large because of the factor N^2 in (4.4a).) Disregarding all higher order terms in (4.6), the three constants $C_\ell(1)$, a and b were determined such that the resulting curve passed through all points (1/N). The agreement between this curve and the calculated points extended down to N=5, far to the right of Fig. 8. The origin of this curve is $C_\ell(1) = 1.5930904...$

This agreement, while it tends to be reassuring, must be somewhat coincidental, however; it is highly unlikely that the higher terms in (4.6) should be negligible down to N=5. Indeed, we should correctly have $a=-D_2$, see (4.5). This condition was not quite fulfilled, and an adjustment had to be made, allowing for small but finite higher order terms in (4.6). The adjustment led to the new value $C_\ell(1) = 1.5930884...$ Both new values are marked in Fig. 8. The smallness of the difference between them may be taken as an indication of the degree of accuracy which had been achieved.

In Table I the value $a_2 = 0.1267740$ is used; to it corresponds $C_\ell(1) = 1.5930890$. In the context of Table I, the number a_2 has to be treated as an exact number; however, the listed value is not claimed to be correct beyond the accuracy range which is indicated by Fig. 8.

(c) Listing of the Solution

The reference set $C_{2\kappa}$ is listed in Table I where it is denoted by $C_{2\kappa,0}$. We discuss first how this table was calculated.

Two successive sets $C_{2\kappa}^{N-1}$ and $C_{2\kappa}^{N}$ differ because of two different reasons. One, the sets $C_{2\lambda+1}^{N-1}$ and $C_{2\lambda+1}^{N}$ differ. Two, the new end term $C_{2\lambda+1}^{N}$ enters in (2.7b) when $C_{2\kappa}^{N}$ is calculated. The second cause has by far the larger effect. Therefore, we wrote for N large

$$C_{2\kappa}^{N} - C_{2\kappa}^{N-1} = \frac{1}{\pi} \frac{2NC_{2N+1}^{N}}{N^2 - \kappa^2}(1-\epsilon) \qquad \text{(times } \tfrac{1}{2} \text{ if } \kappa=0\text{)} \qquad (4.7)$$

The number ϵ is here introduced to take care of reason one.

We found that ϵ changed little with κ and less with N. If one assumes that, as N increases, ϵ remains constant and C^N_{2N+1} behaves like $\log\lambda/\bar{\lambda}^3$ (compare (4.3); the constant D_1 is small in the case of the reference solution) one can sum the differences (4.7) to infinity, and thus obtains $C_{2\kappa}$. Doing this for both N=40 and N=60, we found that our results were the same within our accuracy requirements (the agreement began to deteriorate beyond κ=25 since κ approached N=40, but results beyond κ=25 were not required).

Table I lists $C_{2\kappa}$ up to κ=15, and lists the remainder R_κ which was calculated by means of the listed value a_2. The remainder R_κ is broken down further in the manner shown (I_κ is again the logrithmic set defined by (2.16d)), and a final remainder $\bar{\bar{R}}_\kappa$ is listed in the last column. This column is zero from κ=15 onward.

The constants b_4 and c_4 were determined by means of the three conditions

$$\text{(a) } \bar{\bar{R}}_p = 0 \;;\quad \text{(b) } \sum_0^p \bar{\bar{R}}_\kappa = 0 \;;\quad \text{(c) } \bar{\bar{R}}_\kappa = 0 \text{ for } \kappa > p \qquad (4.8)$$

Here p is a number which has to be determined by trial and error. One chooses p and determines b_4 and c_4, using conditions (a) and (b). The zero sum condition (2.6) must apply to the set $\bar{\bar{R}}_\kappa$ (that is, if both analysis and numerical work are without error) because it applies individually to all other sets in $C_{2\kappa}$. Hence the sum of all $\bar{\bar{R}}_\kappa$ from p+1 to ∞ must be zero when (a) is fulfilled. However, this does not insure that (c) is fulfilled. Rather, if p was chosen too small, the $\bar{\bar{R}}_\kappa$ beyond p will describe a wavy curve about the zero line.

On the other hand, significant decimals are lost, and the constants b_4 and c_4 will be ill-defined, if p is chosen too large. In fact, it is not possible to determine these constants very accurately; though seven decimals are listed in Table I, the last decimals should not be considered reliable. A small change in b_4 and c_4 will affect the first few listed values $\bar{\bar{R}}_\kappa$; however, since these first few values almost cancel each other, the changes will cancel out entirely, and the validity of (4.8) will not be affected.

On the other hand, the fact that it was possible to find p, b_4 and c_4 such that (4.8) was fulfilled to 10 decimals (allowing for rounding-off errors) and that the set $\underline{\underline{R}}_\mu$ converged smoothly and rapidly: this fact can be considered an overall confirmation of analysis and numerical work. (The value p which we used was p=20.)

The set $C_{2\mu,0}$ converges slowly; written out to eight decimals, it would extend to about $\mu = 5,000$. Table I demonstrates that, knowing the structure of the solution, one can store it in form of the short set $\underline{\underline{R}}_\mu$ plus the three numbers a_2, b_4 and c_4. (These numbers have to be treated as exact numbers, of course, when one uses them to reconstruct the set $C_{2\mu,0}$.) The stored numbers contain all the specific information about the specific solution; the bulk of the numbers in the infinite set $C_{2\mu,0}$ describes the general tip singularity.

We close this section on the reference solution by noting also the values $C_{L,0}$ and $\zeta_{L,0}$ which arise by means of (2.4e). They describe the vector of total lift for the planar circular wing. A fair number of approximate values are given in the literature, and some of the differences between these are sizeable. Our results

$$C_{L,0} \approx 1.79002303 \quad ; \quad -\zeta_{L,0} \approx 0.52085758 \tag{4.9}$$

should be reliable to less than one unit in the last decimal given.

5. Calculation of Additional Solutions

(a) Procedure

To engineering accuracy, solutions for a given downwash w(y) are obtained directly from (3.1). If one wants very high accuracy in order to treat more details of the solution, one can make use of the given reference solution $C_{2\mu,0}$ to simplify the numerical procedure. Write instead of (2.16)

$$-C_{2\mu} = -XC_{2\mu,0} + H_\mu \tag{5.1}$$

Here $C_{2\mu,0}$ takes the place of the general set G_μ. In order to insure that the set H_μ plays the role of the remainder R_μ, we have to determine the factor X such that

$$a_2 = Xa_{2,0} \tag{5.1a}$$

The leading set in H_κ is then again $0(\kappa^{-4}\log\kappa)$.

We write H_κ rather than R_κ in (5.1) to indicate that there is a difference. The set R_κ is a remainder; it contains the specific sets which describe the specific solution $C_{2\kappa}$, but it contains also those general sets of higher order which are not listed in the general part of (2.16). On the other hand, the set H_κ is void by definition of all general sets which might be transferable from R_κ into G_κ. The void set H_κ is that specific signature of the given downwash w(y) which distinguishes $C_{2\kappa}$ from $C_{2\kappa,0}$.

The advantage of replacing (2.16) by (5.1) is that it is much easier to determine the factor X than to determine the amplitude a_2. Our numerical procedure corresponded essentially to (4.7). We calculated sets $C^N_{2\kappa}$ and $C^N_{2\kappa,0}$ up to N=60 and determined a preliminary value X by assuming in (5.1) that H^N_κ was negligible for $\kappa \approx N$. This allowed one to calculate H^N_κ and to use it in the place of $C^N_{2\kappa}$ on the left of (4.7). In the term which then corresponds to C^N_{2N+1} on the right of (4.7), the logarithmic term with D_0 from (4.3) has been eliminated by (5.1a), and the rational term with D_1 (no longer small) has become the leading term. This simplifies the summation, and hastens its convergence. The new extrapolative corrections were generally smaller than those of the reference solution.

The results are listed in Table II in a form corresponding to Table I:

$$-C_{2\kappa,nv} = H_\kappa = \frac{1}{\kappa^4}(b_4 L_\kappa + c_4) + \underline{\underline{H}}_\kappa \tag{5.2}$$

Here n is the number of the solution, and the suffix v denotes its void part. To find the amplitudes b_4 and c_4 requires a process corresponding to (4.8). A slight complication arose from the fact that the calculation had started from a preliminary value X. We had to determine the effect of a unit change in X and had to adjust X by linear superposition such that the final set $\underline{\underline{H}}$ converged properly.

(b) Sample Results

If one stores the solutions for a number of linearly independent downwash distributions $w_n(y)$, one can compose the members of a class of solutions as required. A logical choice for the $w_n(y)$ are the Gegenbauer polynomials:

$$w_n(y) = \bar{P}_{2n}(y) \tag{5.3}$$

The corresponding downwash coefficients w_s are from(2.14)

$$w_{n,n} = \left[(n+1)(2n+1)\right]^{-1} ; \quad w_{s,n} = 0 \quad \text{for } s \neq n \tag{5.3a}$$

Our reference solution fits into this system as the case n=0. We calculated in addition the solutions for n=1, 2 and 3. These are listed in Table II.

The downwash $w_n(y)$ is given in Table II in the form

$$w_{n,v}(y) = w_n(y) - X_n \tag{5.4}$$

The complete solution $C_{2\kappa,n}$ is given by

$$C_{2\kappa,n} = X_n C_{2\kappa,0} + C_{2\kappa,nv} \tag{5.5}$$

The void solution $C_{2\kappa,nv}$ is obtained from Table II by means of (5.2).

In the columns of Table II, there is always a sign change between κ=n and κ=n+1. The numerical values in the sets $\bar{\bar{H}}_\kappa$ increase as n increases, and consequently the listed sets become longer. (We used p=25 in (3.10) in all three cases of Table II.)

The void span loadings $C_{\ell,nv}(y)$ which belong to Table II are shown in Fig. 9. They appear to have finite tangents at the tip; however, this has not been investigated closely. An interesting observation of physical interest is the following: one can form the ratio between two integrals over the wing, the total lift and the integral over the downwash momentum. This ratio turned out to be almost invariant between the reference solution and the three individual void solutions of Fig. 9; the maximum variation was less than 1%. It appears that, as far as the total lift is concerned, the details of how the downwash is distributed over the wing span are of negligible

importance; they do not seem to affect the outer flow which determines the total lift.

The ratio varied somewhat more when the complete solutions, Fig. 10, were compared. Small differences between large numbers occurred in the superposition, and the lift-momentum ratio was found to vary from 0.895 for n=0 to 0.821 for n=3.

Shown in Fig. 10 are both the downwash distributions $w_n(y)$ and their span loadings $C_{\ell,n}(y)$. All the latter curves form a downward hook on approaching the wing tip, reaching a vertical tangent at the tip itself. However, on the scale of Fig. 10 this hook is no longer visible when n=2; even though the bulk of the set C_{2k} still represents the tip singularity, the latter now plays a minor role in the span loading curve.

The scale ratio between w_n and $C_{\ell,n}$ in Fig. 10 is so chosen that w_0 and $C_{\ell,0}$ have roughly the same overall magnitude. For $n \neq 0$, the curves are wavy, and the wave amplitudes in $C_{\ell,n}$ are seen to be distinctly smaller than the corresponding amplitudes in w_n. Each amplitude ratio corresponds roughly to the ratio between half-wavelength and wing span. This is what one would expect from either lifting line theory or slender wing theory; according to either, the lift coefficient becomes proportional to the aspect ratio when the latter becomes small enough, in agreement with our observation, supposing only that one can interpret the length of a half-wave as an effective wing span. That one can do this (roughly) is not entirely unexpected, but it is of interest to see the point verified.

Lifting line theory overpredicts (at small aspect ratios) by the factor 2. This is illustrated for n=3 in Fig. 11. Thus Fig. 11 implies that the correct result corresponds closely to what we would expect from slender wing theory for n=3. On the other hand, there is no slender wing type analysis available to handle the case n=3. A collocation analysis for n=3 would be feasible but would be rather cumbersome and would not necessarily be considered reliable. How many chordwise modes would one have to use with spanwise waves this short? From this point

of view, and in view of the distinct difference in the character of the chordwise distributions in (2.2), it becomes of interest to take a look also at the pressure distributions. This we will do in Section 7.

6. Alternative Elements

An alternative to the set $w_n(y)$ is the set λ^* which was defined in (2.9). If one sets $\widehat{\pi C}_{2\lambda^*+1} = w_{n,n}$, then two corresponding elements $\lambda^*=n$ differ by the effect of S_1 according to (2.15) resp. by the contribution of $\bar{c}^s_{\lambda^*}$ according to (3.1). For the element λ^*, the set $C_{2\kappa}$ is immediately given by (2.7b). The downwash w(y) which belongs to λ^* does not fulfill the tip condition; on the other hand, we saw in Fig. 10 that the tip singularity becomes less and less visible as n increases, and it is illustrated by Fig. 12 that the two elements become increasingly more equal over an increasing range of the wing span.

The downwash distributions λ^*, calculated by means of (3.1) and (2.14), are shown as full lines in Fig. 12. All λ^* curves turn down to $w(1)=-\infty$ but, since the downward turn occurs closer and closer to the tip as λ^* increases, a finite limit value w(1-0) is built up with an infinite number of elements λ^*. Also shown are (as dashed lines) the distributions $w_n(y) = \bar{\bar{P}}_{2n}$; there is a noticeable difference between the two elements when n=0, a small difference when n=1, and no visible difference (except directly at the tip; not shown) when $n \geq 2$.

The set λ^* can be useful because of its analytical simplicity if one wants to investigate, for example, the local effect of a disturbance or discontinuity in w(y) on the inner part of the wing span. In such a problem the higher w_s plays the important role, and for these the local difference between the two sets of elements becomes entirely negligible. Analytically the two sets differ, of course, in that the λ^* elements do not exhibit the complications of (2.16); however, (2.16) describes the tail behavior which produces the proper tip singularity in the n-elements. The amplitudes $C_{2\kappa}$ and $C_{2\lambda+1}$ with $\kappa,\lambda \approx s$ are those which essentially desribe the local pressure distribution, and these hardly different between the two types of elements.

7. Pressure Distribution

The pressure distributions in Figs. 13 and 14 represent the cases $\lambda^*=1$ and $\lambda^*=3$ but would not look noticeably different if they would represent the cases n=1 and n=3.

Like Fig. 2, Figs. 13 and 14 show relief diagrams of $\bar{p}$ over the right half of the circular wing. The left half of the wing is not shown in Fig. 13; it is shown in Fig. 14 to exhibit the wavy distribution of the wing incidence. In both figures, the left wing half is stretched into a rectangle for better visibility of $\bar{p}$; furthermore, the rectangle is cut apart at y=0.9. The finite chord at the wing tip which is produced by the stretching operation exhibits the kinked-linear character of the chordwise distribution at the tip.

Part of a vertical plane through the stretched leading edge is shown by a line of constant $\bar{p}$ (the scales of $\bar{p}$ in the two figures are arbitrary) and by vertical lines of constant y.

The most striking insight of technical interest from Figs. 13 and 14 is that the waviness of w(y), while well reflected in $\bar{p}_{l.e.}$ in accordance with (2.9a), has disappeared almost over the rear part of the wing in Fig. 13, and completely in Fig. 14. This stabilizing effect is the cause for the smallness of the wave amplitudes in $C_{\ell,n}$ in Fig. 10. However, it is of more general interest; while it is shown here on idealized models, it must be of significance for the influence of any disturbances of short spanwise extension.

The chordwise distributions of $\bar{p}$ in Fig. 14 are not kinked (except, of course, at the tip itself) but they are fairly complicated curves. It had been shown in Ref. 8 that for the planar circular wing (n=0) already two Birnbaum-Glauert chordwise modes yield an excellent approximation. For the case n=3, only two modes (i.e., approximation by a parabola) would clearly be insufficient.

To the degree that we can interchange $\lambda^*=3$ and n=3, the difference between the complicated distribution Fig. 14 and the reference distribution Fig. 2 is

contained in the column $C_{2\kappa,\,3v}$ of Table II. This remark illustrates how the bulk of the complete set $C_{2\kappa}$ describes essentially the tip singularity, while the details of $\bar{p}$ over the inner part of the wing are fully contained in the much more rapidly converging void set $C_{2\mu,\,v}$.

8. Conclusion

Since the nature of the pressure singularity at a parabolic wing tip, and in particular all required details of the structure of exact solutions for circular wings, are now known, it has become possible to use numerical results with confidence. One knows about their convergence behavior and can match with the asymptotic wing tip solution. A simple procedure for calculating numerical solutions for the circular wing is described. It is so far specialized to symmetric downwash distributions without camber but could be generalized to deal, for example, with an axisymmetric fan-in-wing configuration.

Four sample solutions have been calculated to very high accuracy and have been tabulated. The solving sets converge slowly; their bulk describes the tip singularity, typified by the solution for the planar wing. This has been split off; the specific solutions which remain are void of the tip singularity and converge rapidly. The sample solutions exhibit details of the mechanism of lifting flow which are of technical interest.

The numerical technique which is described in this paper allows one to investigate, for example, the pressure distribution which arises from a local disturbance or discontinuity in the downwash. In such a problem approximation by means of the alternative elements of Section 6 may be useful, since this approximation becomes increasingly correct with higher order (i.e., s large) effects and since its analytical simplicity may allow analytical treatment of the given problem.

REFERENCES

1. Kinner, W., "Die kreisförmige Tragfläche auf potentialtheoretischer Grundlage", Ingenieur-Archiv Vol. 8, No. 1, Feb. 1937, pp. 47-80.

2. Jordan, P. F., "The Parabolic Wing Tip in Subsonic Flow", AIAA Paper No. 71-10 (Jan. 1971).

3. Jordan, P. F., "Span Loading and Wake Formation", in "Aircraft Wake Turbulence and its Detection", Plenum Press, New York-London, 1971, pp. 207-227.

4. Jordan, P. F., "On Lifting Wings With Parabolic Tips". Paper submitted for publication (July 1971).

5. Jordan, P. F., "A Reversible Transformation and Related Sets of Legendre Coefficients". Paper submitted for publication (July 1972).

6. Abramowitz, M., and Stegun, I. A., ed., Handbook of Mathematical Functions", National Bureau of Standards, 3rd printing 1965.

7. Zandbergen, P. J., Labrujere, Th. E., and Wouters, J. G., "A New Approach to the Numerical Solution of the Equation of Subsonic Lifting Surface Theory", NRL TR G. 49, Nov. 1967.

8. Jordan, P. F., "Remarks on Applied Lifting Surface Theory", Jahrbuch 1967 der WGLR, 1968, pp. 192-210.

κ	$C_{2\kappa,0}$	R_κ	$\bar{R}_\kappa$
0	+.22375288	-.04654659	+.00184543
1	-.14455778	+.04313858	-.00148142
2	-.03065010	+.00255042	-.00030011
3	-. 1349032	+. 52375	-. 4664
4	-. 761010	+. 17088	-. 1125
5	-. 489108	+. 7158	-. 355
6	-. 340778	+. 3510	-. 134
7	-. 251341	+. 1919	-. 57
8	-. 192964	+. 1137	-. 27
9	-. 152820	+. 716	-. 13
10	-. 124027	+. 473	-. 7
11	-. 102674	+. 325	-. 4
12	-. 86400	+. 231	-. 2
13	-. 73712	+. 168	-. 1
14	-. 63628	+. 125	-. 1
15	-. 55481	+. 96	($\kappa \geq 15$) 0

$$-C_{2\kappa,0} = \left[\frac{4}{\kappa(4\kappa+1)} - \frac{3\log^2\kappa}{16\pi^2\kappa^4}\right]a_2 + R_\kappa$$

$$R_\kappa = \frac{1}{\kappa^4}(b_4 L_\kappa + c_4) + \bar{R}_\kappa$$

$a_2 = 0.1267740$
$b_4 = 0.0029655$
$c_4 = 0.0416545$

Table I. Planar Solution ($w(y) \equiv 1$)

κ	$C_{2\kappa,1v}$	$\bar{\bar{H}}_\kappa$	$C_{2\kappa,2v}$	$\bar{\bar{H}}_\kappa$	$C_{2\kappa,3v}$	$\bar{\bar{H}}_\kappa$
0	-.08355512	+.20721931	-.05930497	+.30776604	-.04502880	+.43750001
1	+.10240765	-.21639945	+.04670161	-.27618971	+.03210567	-.39520727
2	-.01601144	+.00870664	+.02349934	-.03789344	+.00938151	-. 3174875
3	-.00186437	+. 40098	-.00856274	+.00571340	+.01056414	-. 1494365
4	-. 52361	+. 5546	-. 37425	+ 47133	-.00519578	+. 381883
5	-. 20553	+. 1224	-. 46234	+ 9207	-. 98681	+. 42559
6	-. 9737	+. 355	-. 20422	+ 2548	-. 37073	+. 10118
7	-. 5216	+. 124	-. 10521	+ 865	-. 17716	+. 3217
8	-. 3048	+. 49	-. 6001	+ 337	-. 9684	+. 1211
9	-. 1902	+. 22	-. 3633	+ 145	-. 5786	+. 510
10	-. 1248	+. 10	-. 2389	+ 67	-. 3686	+. 233
11	-. 854	+. 5	-. 1620	+ 33	-. 2466	+. 113
12	-. 604	+. 3	-. 1138	+ 17	-. 1716	+. 57
13	-. 439	+. 2	-. 823	+ 9	-. 1232	+. 30
14	-. 327	+. 1	-. 610	+ 5	-. 908	+. 16
15	-. 249	+. 1	-. 462	+ 3	-. 685	+. 9
16	-. 192	($\kappa \geq 16$) 0	-. 357	+ 1	-. 526	+. 5
17			-. 280	+ 1	-. 411	+. 3
18			-. 222	($\kappa \geq 18$) 0	-. 326	+. 1
19					-. 262	+. 1
20					-. 213	($\kappa \geq 20$) 0
a_2	= 0		= 0		= 0	
b_4	= 0.0086548		= 0.0024522		= -0.0156775	
c_4	= 0.1053370		= 0.2270359		= 0.3787791	

Table II. Void Solutions $C_{2\kappa,nv}$ (n = 1, 2 and 3)

$$w_{1,v}(y) = (5y^2 - 1)/4 - 0.4324159$$

$$w_{2,v}(y) = (21y^4 - 14y^2 + 1)/8 - 0.2795066$$

$$w_{3,v}(y) = (429y^6 - 495y^4 + 135y^2 - 5)/64 - 0.20268387$$

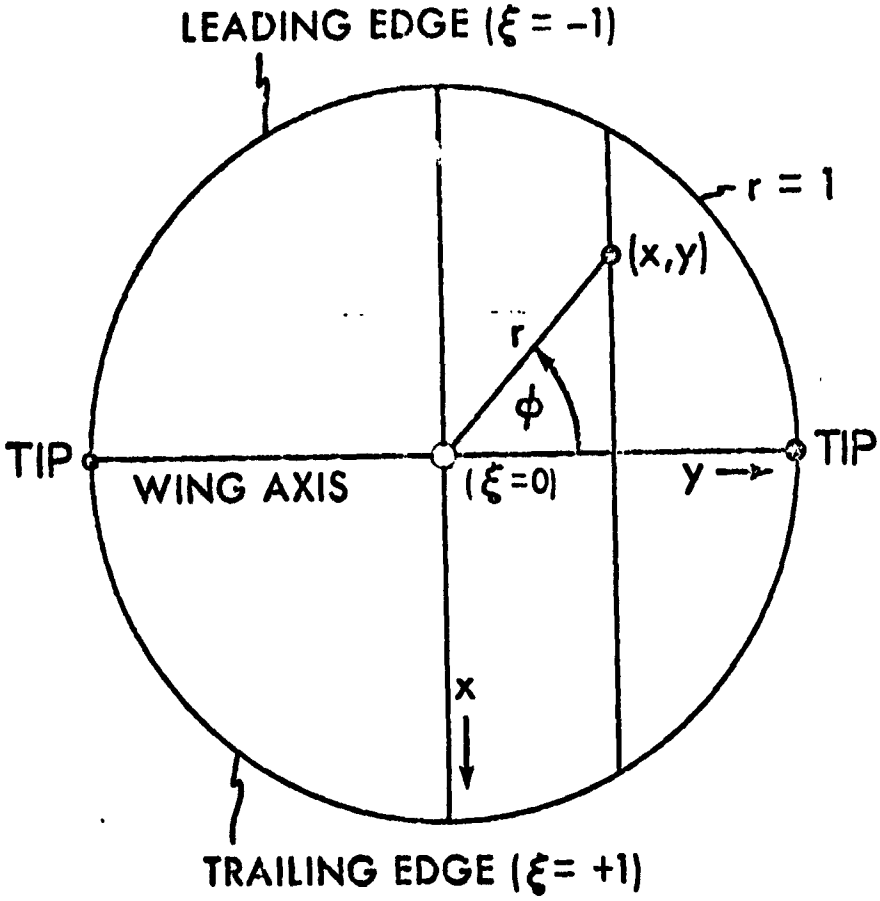

$$\xi = x/\tilde{y} \quad ; \quad \tilde{y} = (1-y^2)^{1/2}$$

Fig. 1. Coordinates and Notation

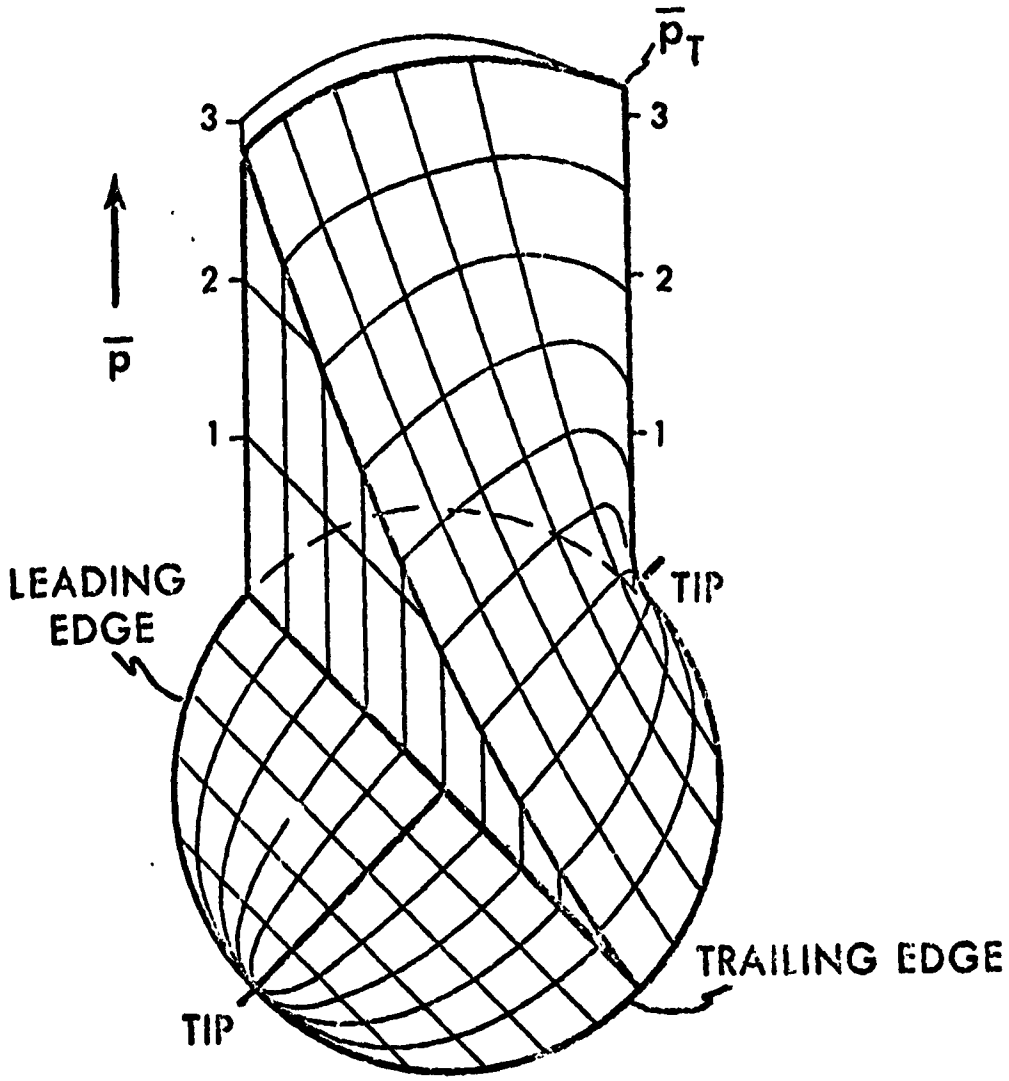

Fig. 2. Relief of Pressure Function over One-half of Planar Wing

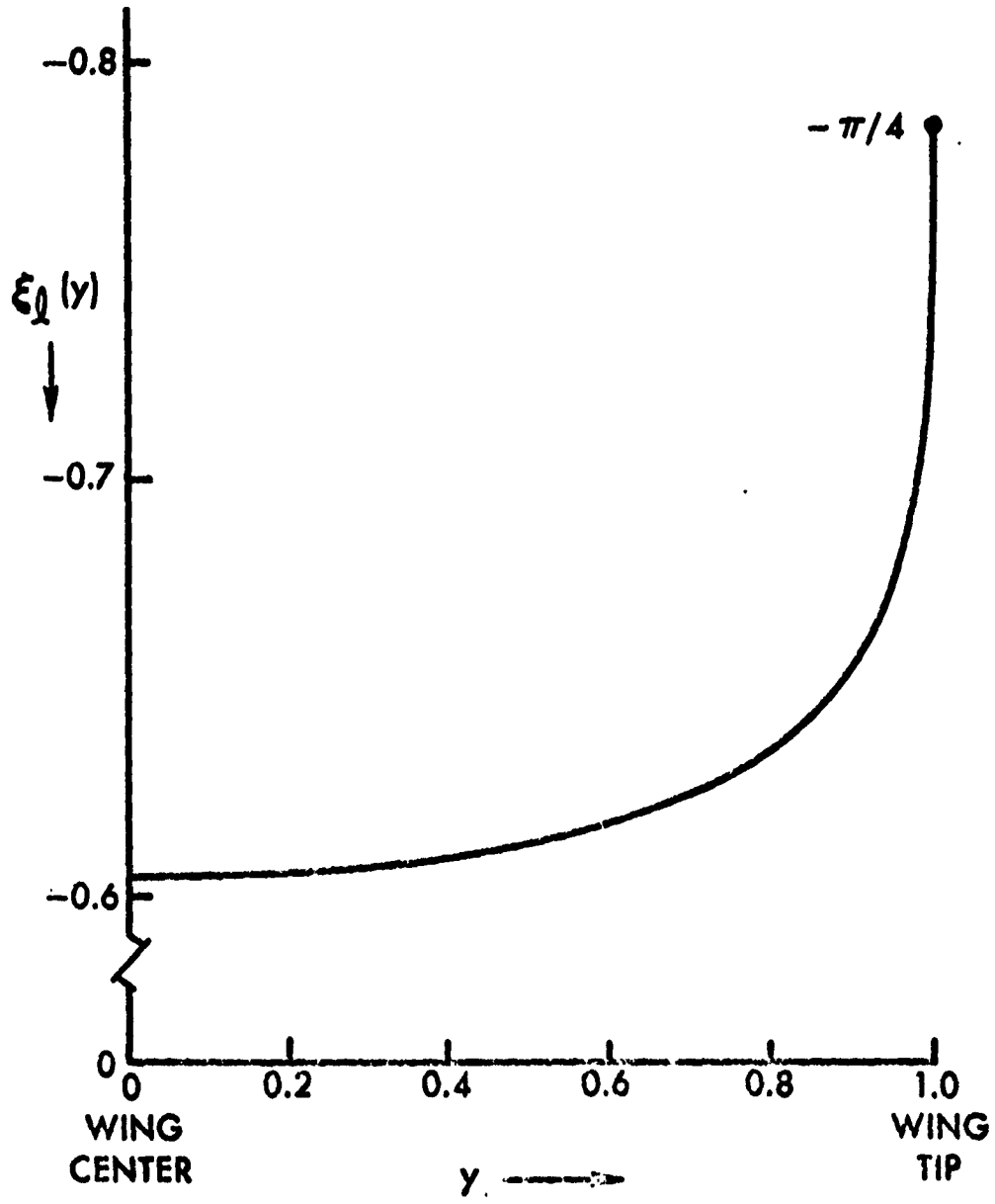

Fig. 3. Chordwise Position of Center of Pressure

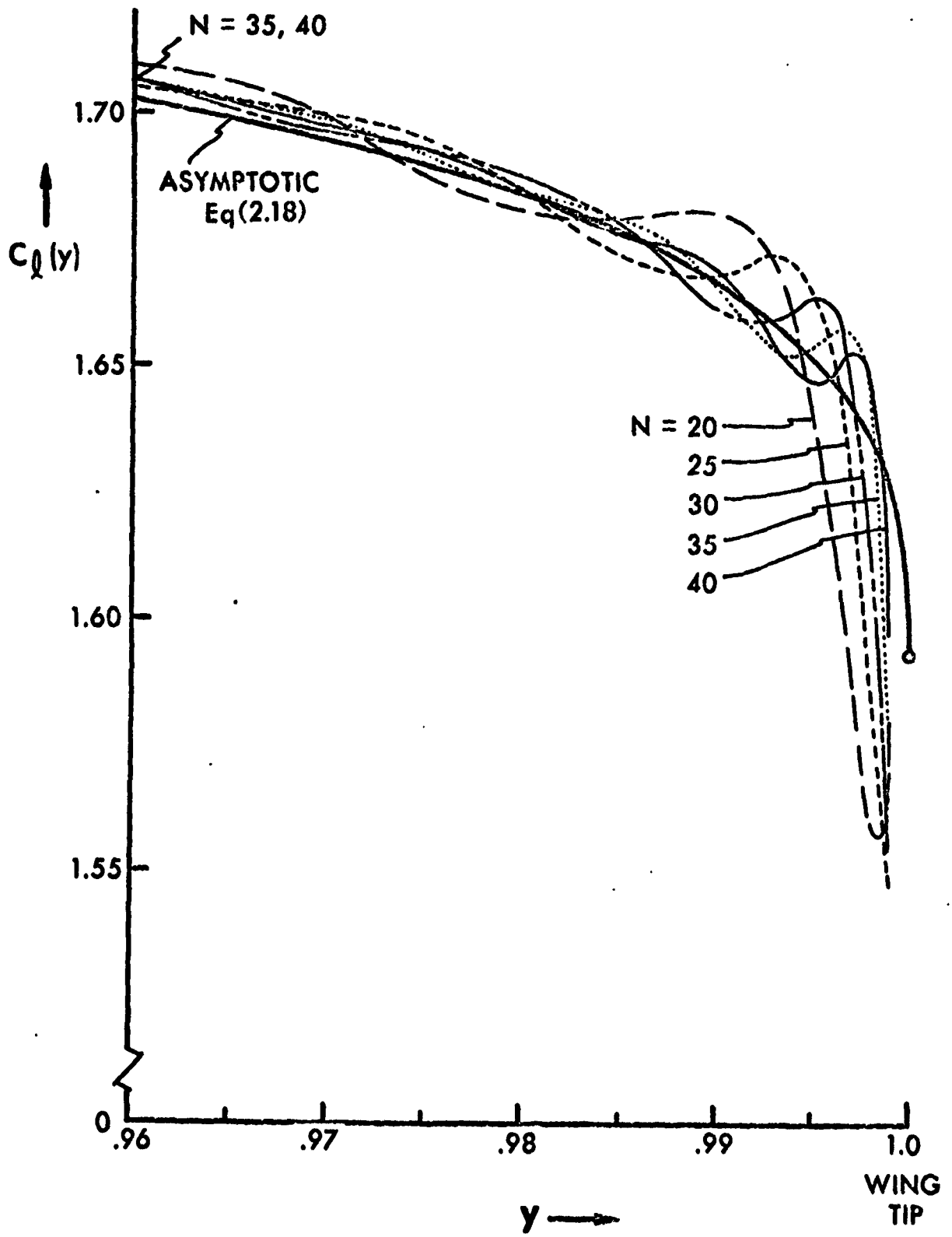

Fig. 4. Convergence of Legendre Series near Wing Tip

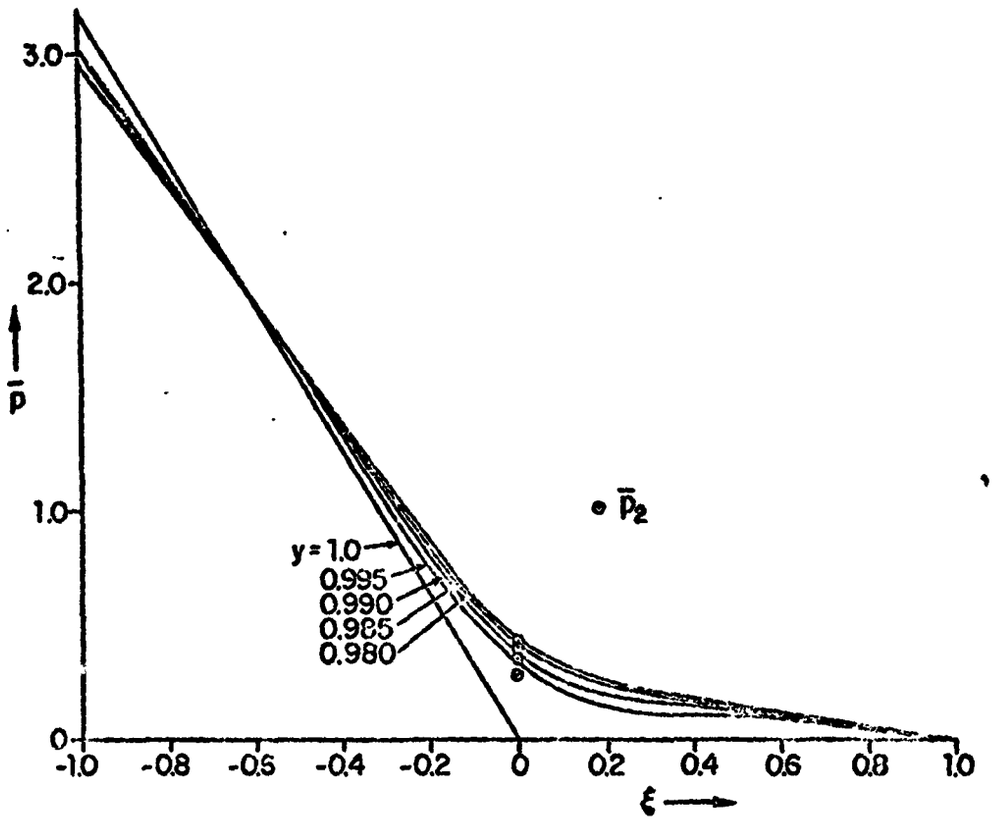

Fig. 5. Chordwise Pressure Distribution Functions near Wing Tip

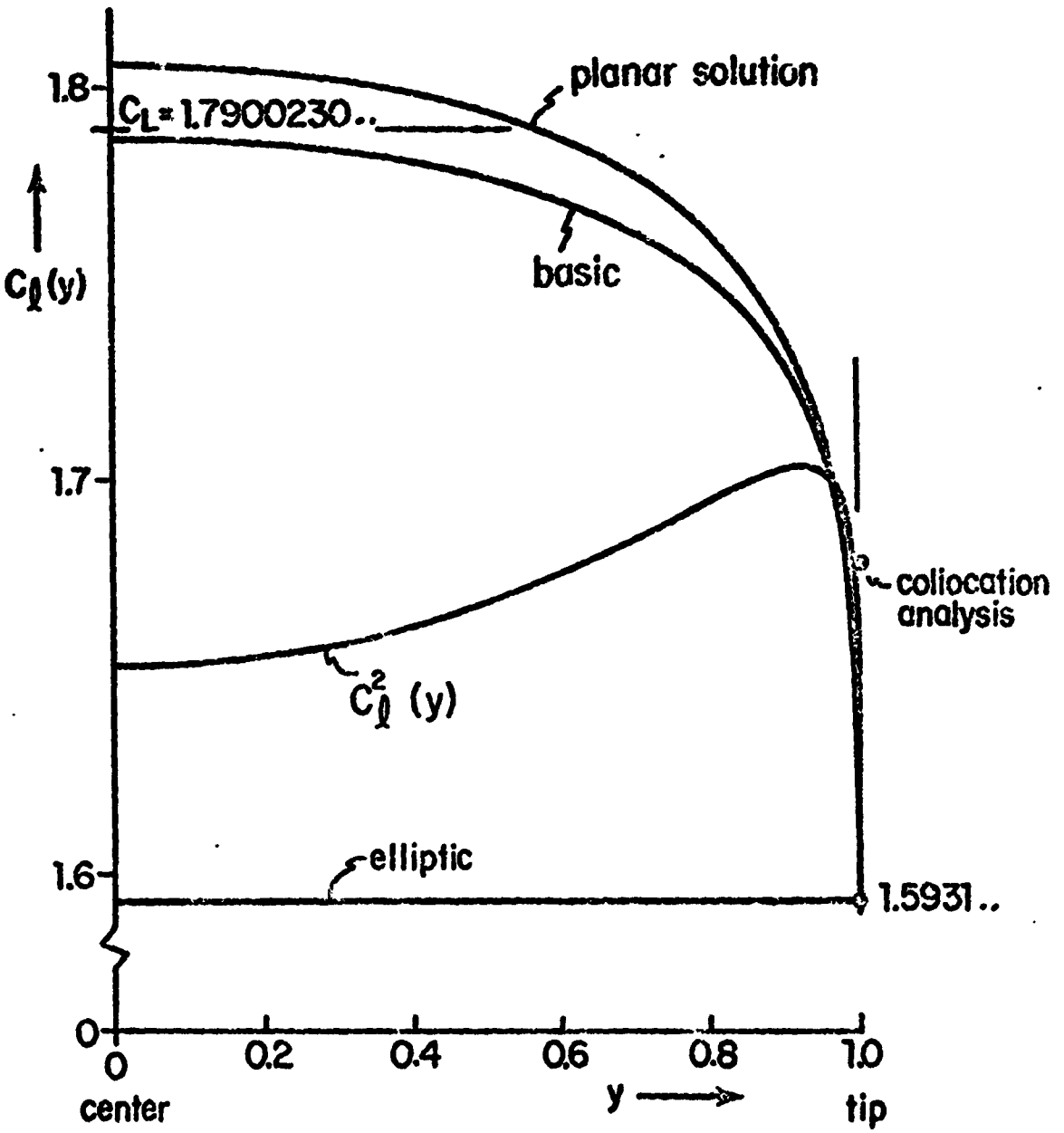

Fig. 6. Lift Coefficient over Planar Wing

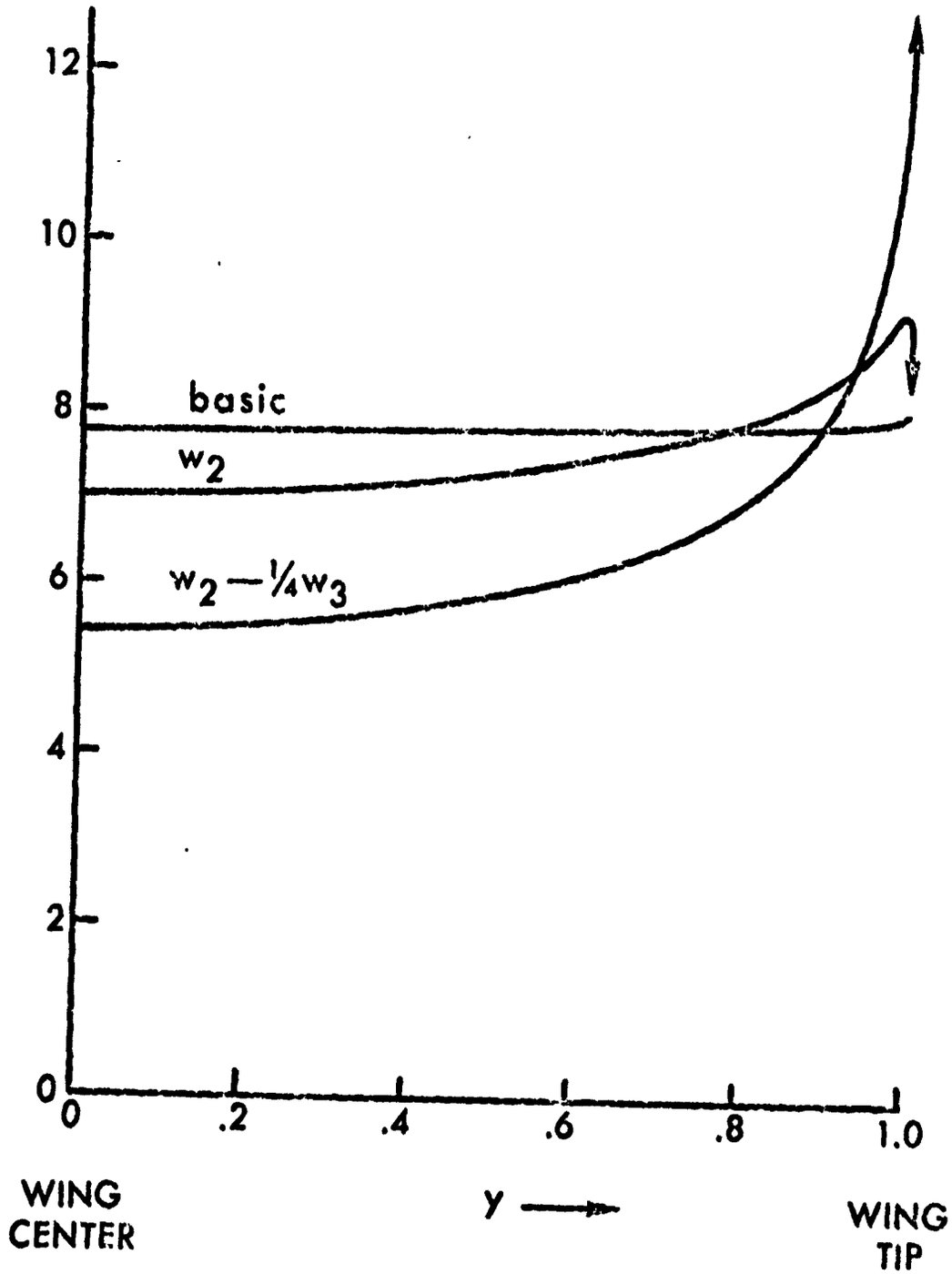

Fig. 7. Elementary Downwash Distributions

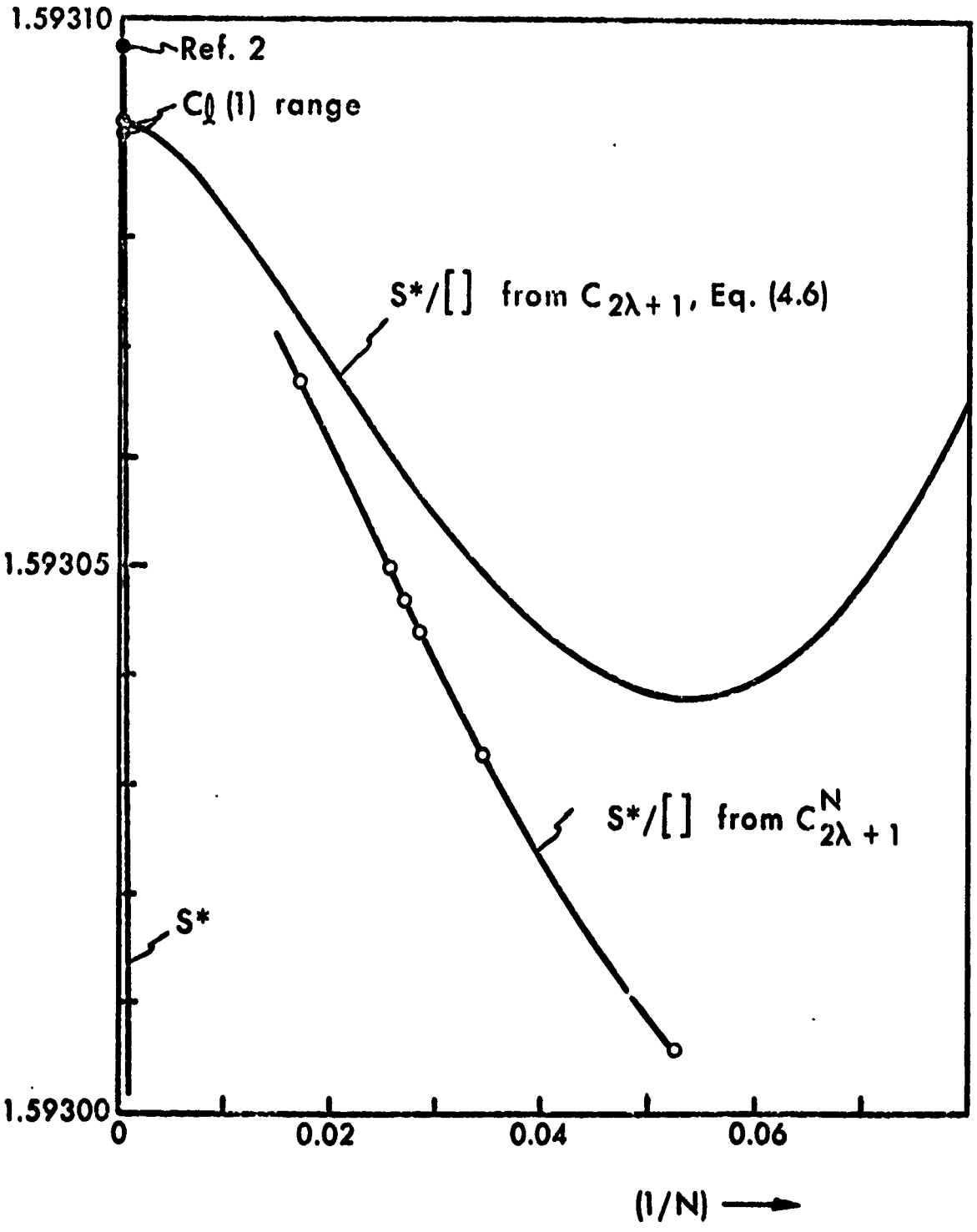

Fig. 8. Extrapolation to Determine $C_\ell(1)$

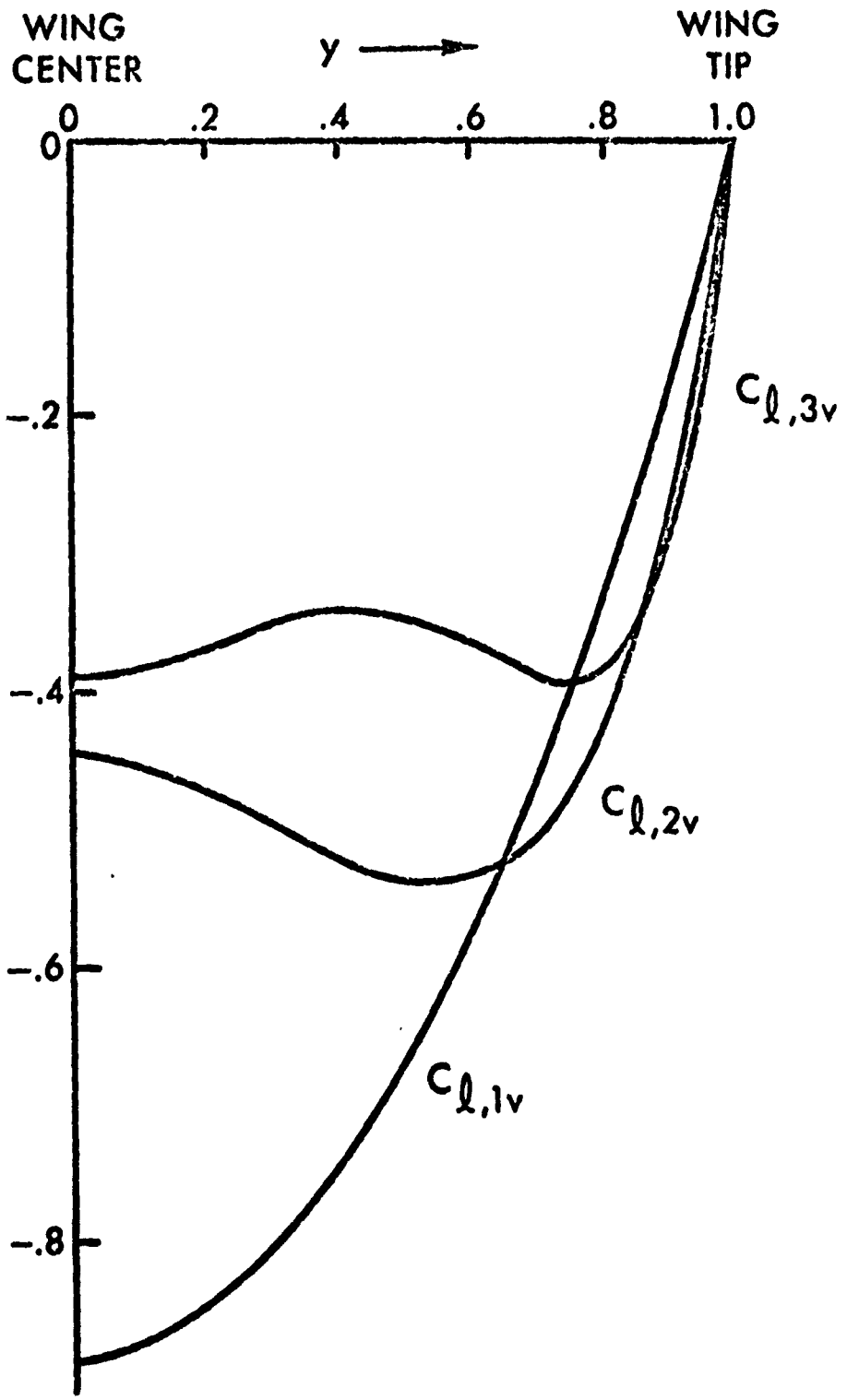

Fig. 9. Void Span Loadings $C_{\ell,nv}(y)$

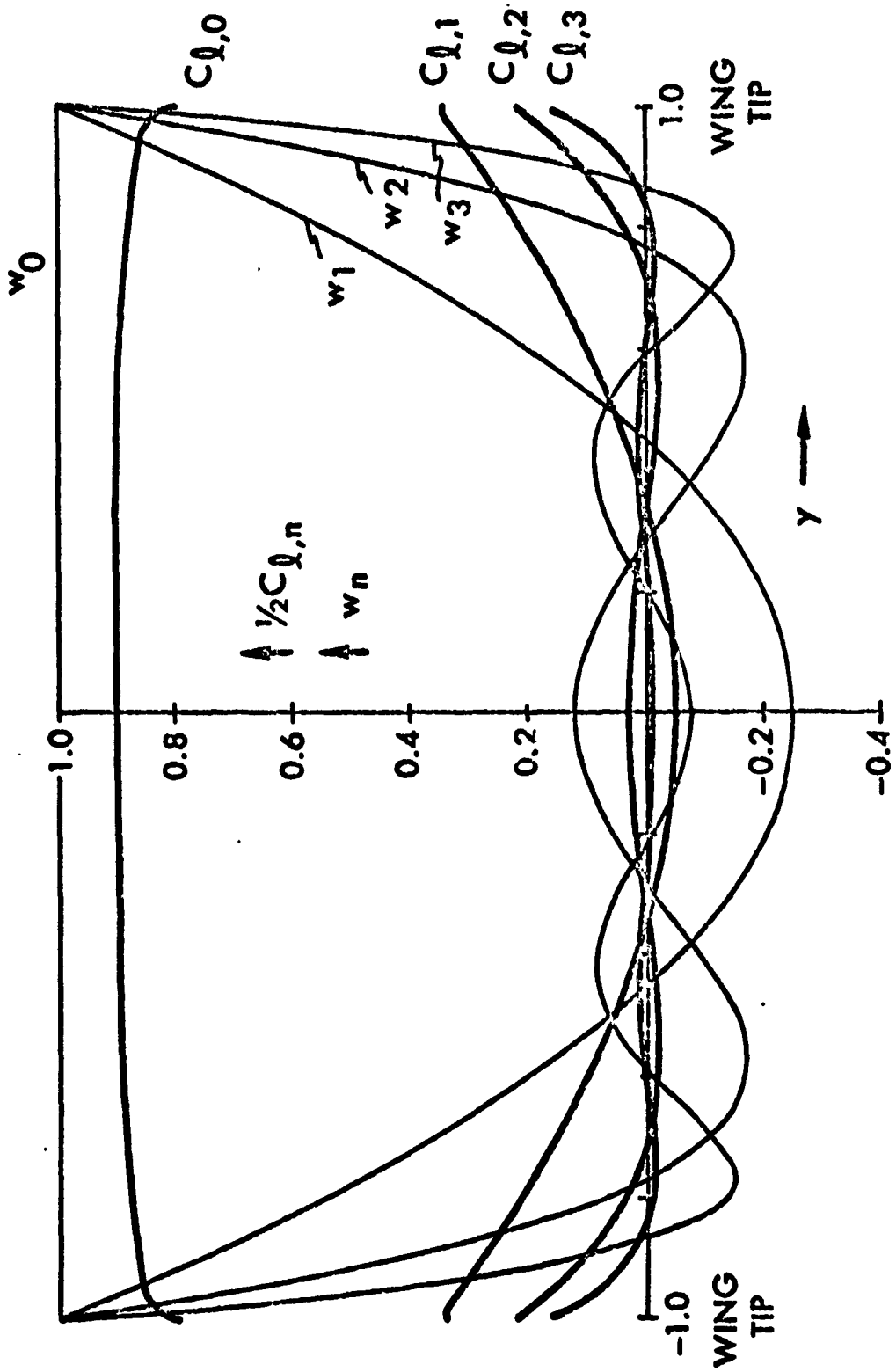

Fig. 10. Span Loadings $C_{\ell,n}(y)$

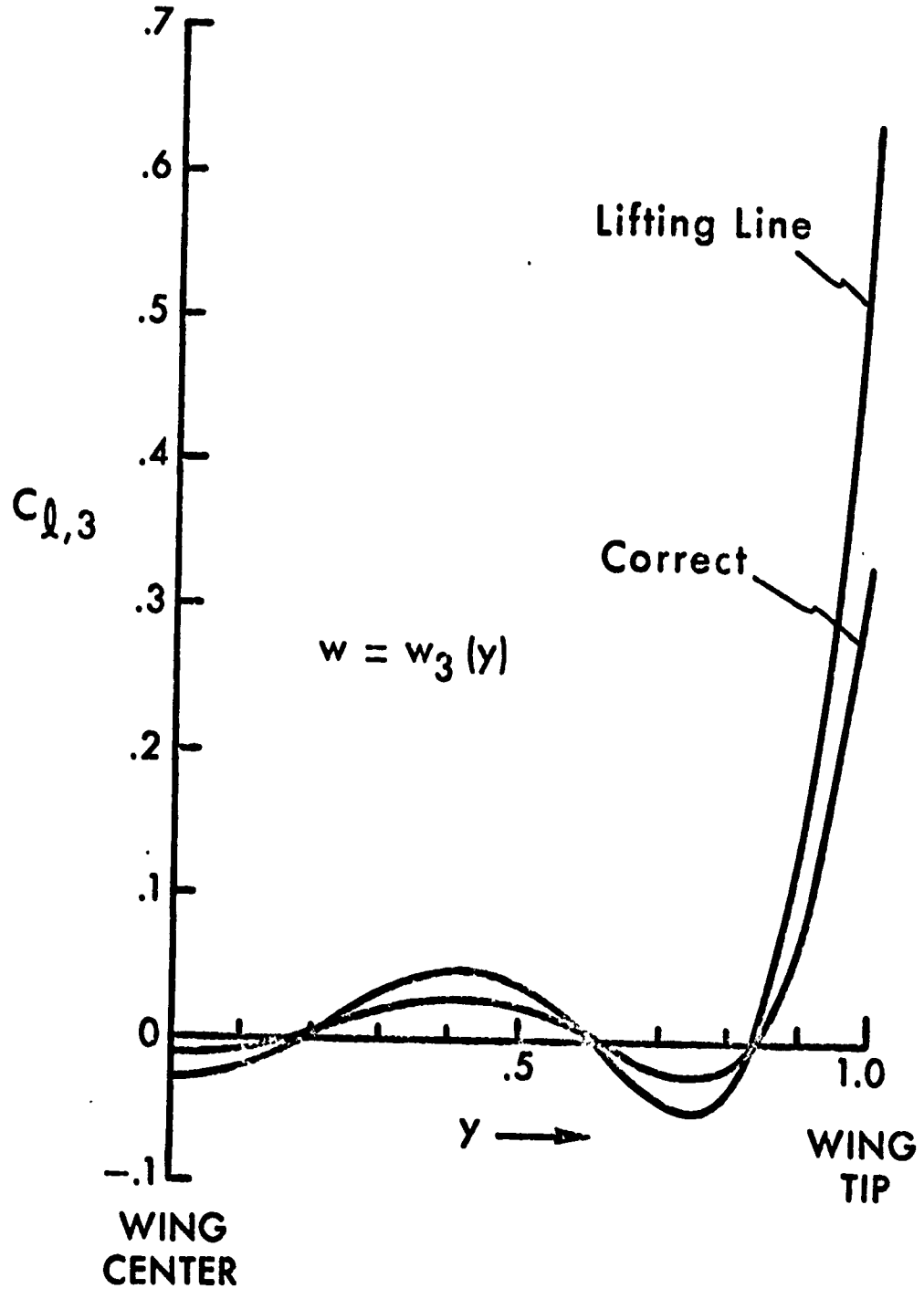

Fig. 11. Comparison of Lifting Line Result with Exact Solution

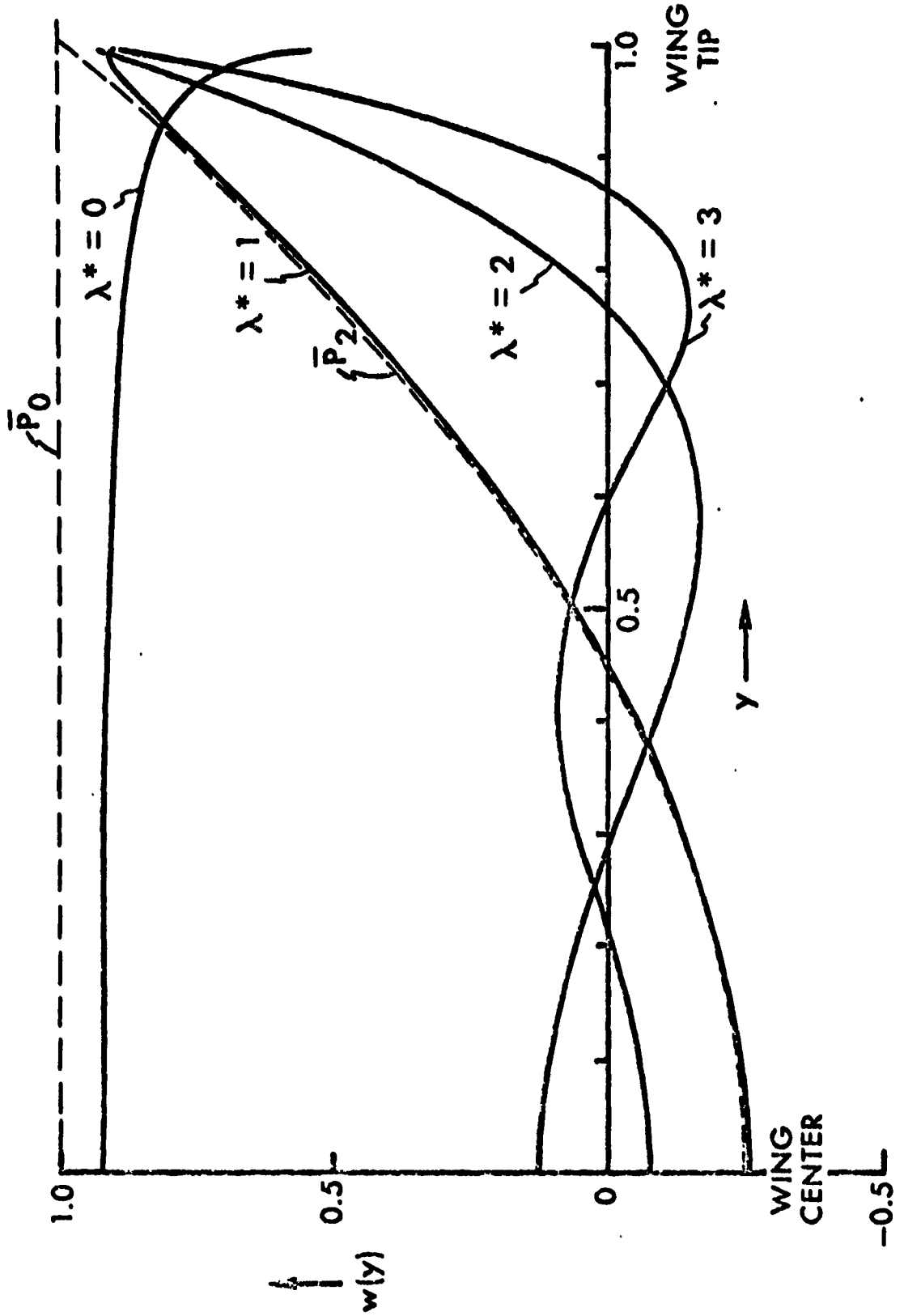

Fig. 12. Downwash Distributions λ^*

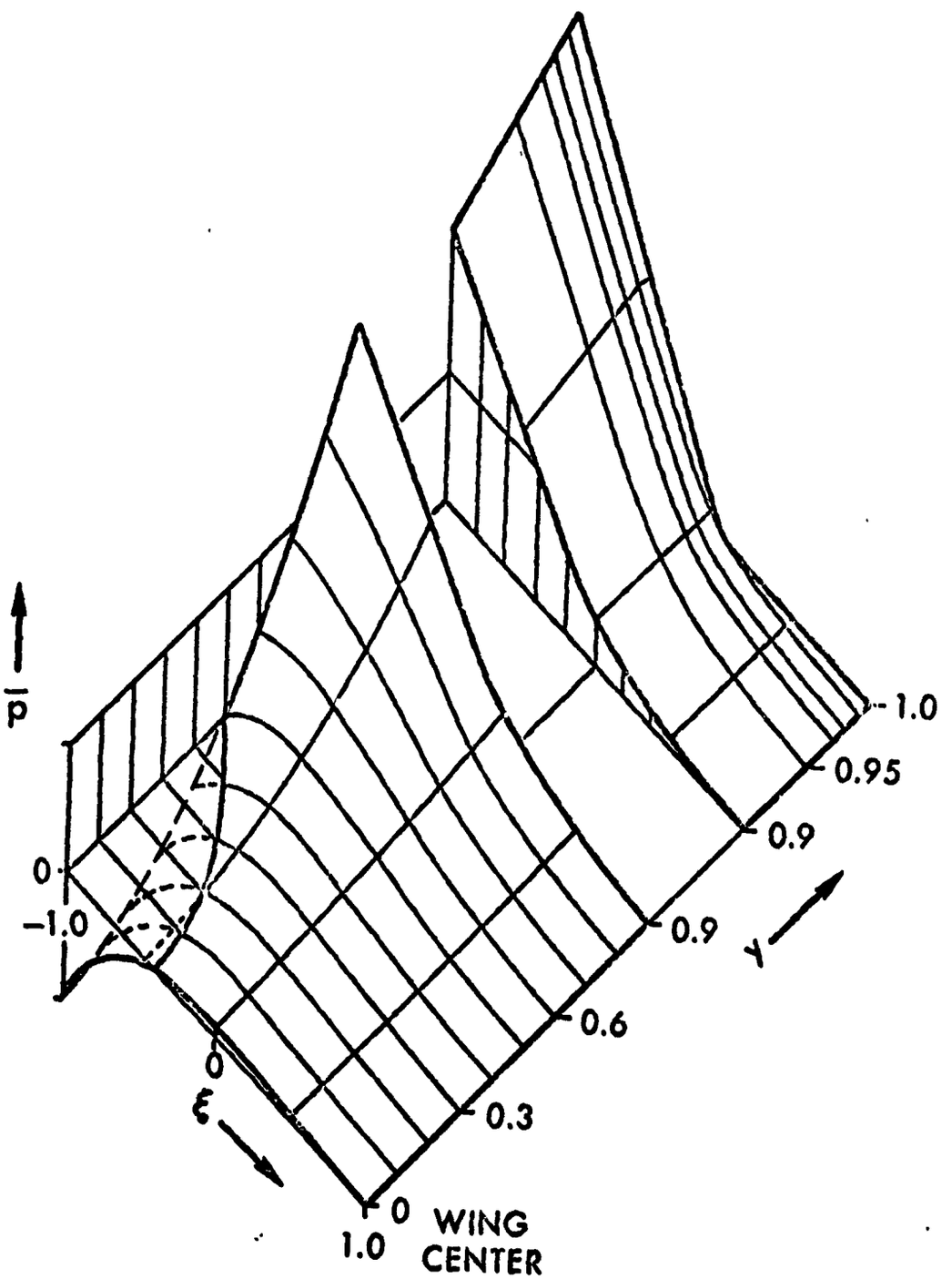

Fig. 13. Pressure Function for $\lambda^* = 1$

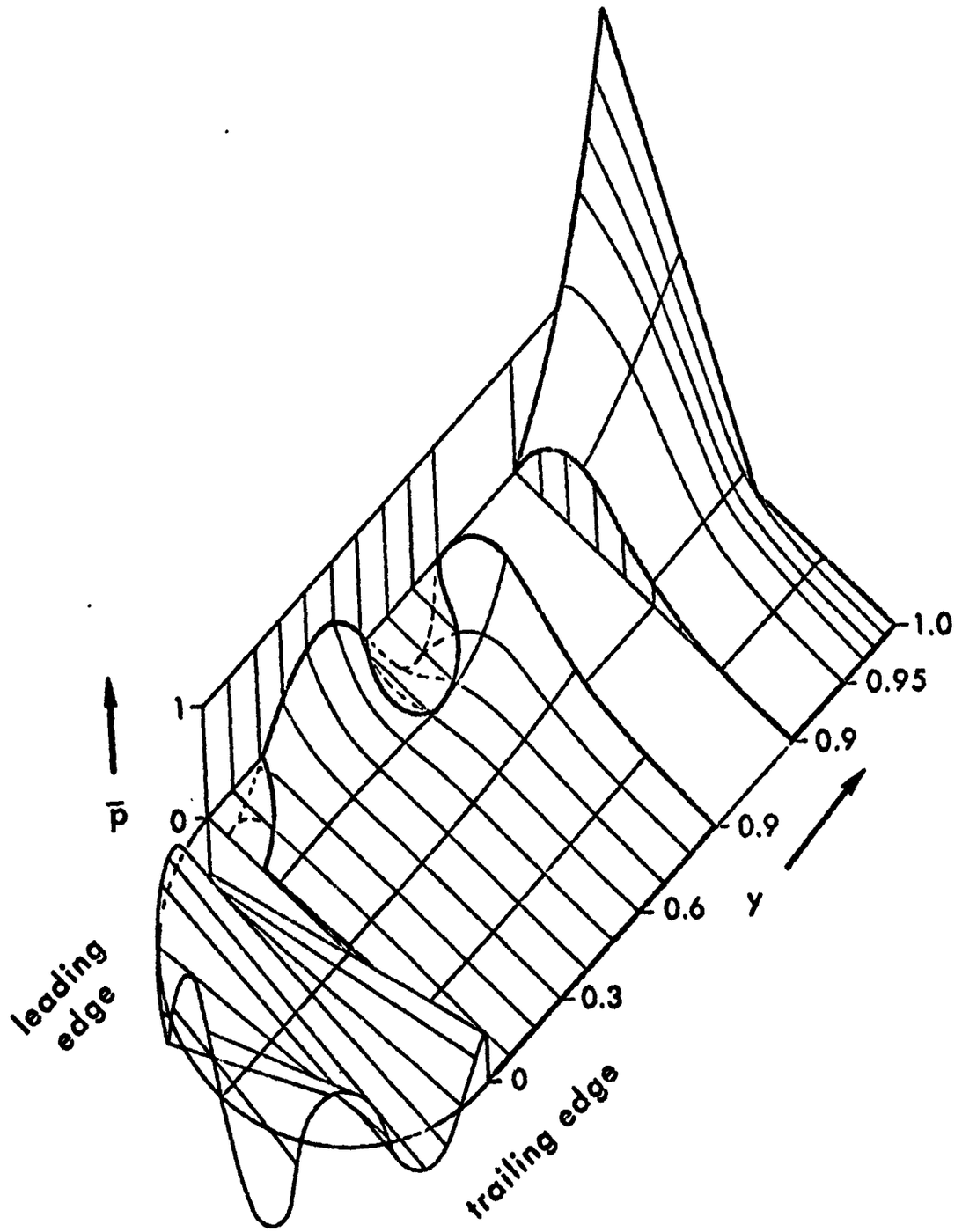

Fig. 14. Pressure Function for $\lambda^* = 3$

APPENDIX

INFINITE SUMS

All the elementary sets E_κ from which the solving set $C_{2\kappa}$ is built up obey the zero sum condition (2.6); the leading element E_0 is thus given by

$$E_0 = -\sum_{\kappa=1}^{\infty} E_\kappa \tag{A.1}$$

Since the E_κ are reciprocal progressions, the rate of convergence of the sum slows down indefinitely as κ increases, and numerical term-by-term summation is not usually a practical proposition.

Some of the required sums are tabulated, see e.g. (2.10) for the rational sets E_κ^r. For the first set in (2.16) we have from 6.3.16 of Ref. 6

$$\sum_1^{\infty} \frac{4}{\kappa(4\kappa+1)} = 4\left[\psi(5/4) + \gamma\right] = 1.399048526.. \tag{A.2}$$

Certain sums involving L_κ are derived in Ref. 5; for example

$$\sum_1^{\infty} \frac{L_\kappa}{\kappa^2} = 7\zeta(3)/4 = 2.103599581 \tag{A.3a}$$

and

$$\sum_1^{\infty} \frac{L_\kappa}{\kappa^4} = \left[31\zeta(5) - 14\zeta(2)\zeta(3)\right]/4 = 1.115624875.. \tag{A.3b}$$

The sum (A.3b) occurs in Tables I and II. The sum (A.3a) occurs in the leading term of $C_{2\lambda+1}$, see (2.16c).

When tabulations are not available, one can use the formula

$$\sum_{N+1}^{\infty} E_\kappa = \int_N^{\infty} E(x)dx - \frac{1}{2}E_N - \frac{1}{12}\left(\frac{dE(x)}{dx}\right)_{x=N} + \ldots \tag{A.4}$$

to calculate the tail sum. Equation (A.4) assumes that E_κ converges smoothly and that the function $E(x)$ interpolates E_κ such that $E(\kappa) = E_\kappa$. Equation (A.4)

was used for example for the extrapolations based on (4.7).

For the term with $\log^2 n$ in (2.16) one requires the sum

$$\sum_1^\infty \frac{\log^2 n}{n^4} = 0.06505816.. \qquad \text{(A.5)}$$

which was determined by means of (A.4).